General Disclaimer

One or more of the Following Statements may affect this Document

- This document has been reproduced from the best copy furnished by the organizational source. It is being released in the interest of making available as much information as possible.

- This document may contain data, which exceeds the sheet parameters. It was furnished in this condition by the organizational source and is the best copy available.

- This document may contain tone-on-tone or color graphs, charts and/or pictures, which have been reproduced in black and white.

- This document is paginated as submitted by the original source.

- Portions of this document are not fully legible due to the historical nature of some of the material. However, it is the best reproduction available from the original submission.

NASA TECHNICAL MEMORANDUM

NASA TM X-73486

NASA TM X-73486

(NASA-TM-X-73486) DESIGN AND PERFORMANCE EVALUATION OF SMALL, TWO- AND FOUR-STAGE DEPRESSED COLLECTORS FOR A 4.8 TO 9.6 GHz HIGH-PERFORMANCE TRAVELING WAVE TUBE Interim Report, Apr. 1975 - Jun. 1976 (NASA) G3/33

N76-30444
HC $4.50

Unclas
49563

DESIGN AND PERFORMANCE EVALUATION OF SMALL, TWO- AND FOUR-STAGE DEPRESSED COLLECTORS FOR A 4.8 TO 9.6 GHz HIGH-PERFORMANCE TRAVELING WAVE TUBE

Peter Ramins, Henry G. Kosmahl, and Thomas A. Fox
Lewis Research Center
Cleveland, Ohio 44135

August 1976

1. Report No.	2. Government Accession No.	3. Recipient's Catalog No.
NASA TM X-73486		

4. Title and Subtitle	5. Report Date
DESIGN AND PERFORMANCE EVALUATION OF SMALL, TWO- AND FOUR-STAGE DEPRESSED COLLECTORS FOR A 4.8- TO 9.6-GHz, HIGH-PERFORMANCE TRAVELING WAVE TUBE	July 1976
	6. Performing Organization Code
7. Author(s)	8. Performing Organization Report No.
Peter Ramins, Henry G. Kosmahl, and Thomas A. Fox	E-8873
	10. Work Unit No.
9. Performing Organization Name and Address	11. Contract or Grant No.
Lewis Research Center National Aeronautics and Space Administration Cleveland, Ohio 44135	
	13. Type of Report and Period Covered
12. Sponsoring Agency Name and Address	Technical Memorandum
National Aeronautics and Space Administration Washington, D. C. 20546	14. Sponsoring Agency Code

15. Supplementary Notes

Interim report, April 1975-June 1976. Prepared for U.S. Air Force, Air Force Systems Command/Aeronautical Systems Division, Deputy for Engineering, Directorate of Avionics Engineering, Wright Patterson Air Force Base, Ohio. Donald E. Laycock, Project Engineer.

16. Abstract

In a joint USAF-NASA program, the Lewis Research Center is carrying out a program to improve the efficiency of traveling wave tubes (TWT's) for use in electronic countermeasure (ECM) systems by applying multistage-depressed-collector (MDC) and spent-beam refocusing techniques developed at Lewis. Three-dimensional electron trajectories are computed throughout the slow-wave structure of the TWT, the spent-beam refocuser, and the depressed collector. Both TWT and MDC performances are analytically evaluated. The experimental program consists of TWT performance evaluation, refocusing system performance evaluation, and MDC performance evaluation. Experimental results have yielded MDC efficiencies of 81 to 83 percent for a two-stage MDC over the full octave bandwidth and 83.6 to 85 percent for a four-stage MDC.

17. Key Words (Suggested by Author(s))	18. Distribution Statement
Traveling wave tube; TWT efficiency enhancement; Depressed collectors; Beam refocusing; TWT performance analysis	Unclassified - unlimited

19. Security Classif. (of this report)	20. Security Classif. (of this page)	21. No. of Pages	22. Price*
Unclassified	Unclassified		

* For sale by the National Technical Information Service, Springfield, Virginia 22161

DESIGN AND PERFORMANCE EVALUATION OF SMALL, TWO- AND FOUR-STAGE DEPRESSED COLLECTORS FOR A 4.8- TO 9.6-GHz, HIGH-PERFORMANCE TRAVELING WAVE TUBE

by Peter Ramins, Henry G. Kosmahl, and Thomas A. Fox

Lewis Research Center

E-8873

SUMMARY

In a joint USAF-NASA program, the Lewis Research Center is carrying out a program to improve the efficiency of traveling wave tubes (TWT's) for use in electronic countermeasure (ECM) systems by applying multistage-depressed-collector (MDC) and spent-beam refocusing techniques developed at Lewis. In the analytical part of the effort, three-dimensional electron trajectories are computed throughout the slow-wave structure of the TWT (10 to 18 percent electronic efficiency, 4.8- to 9.6-GHz) bandwidth, and 330- to 550-W continuous-wave power output). Trajectory computation continues through the spent-beam refocuser and the depressed collector. Collector efficiency, collector losses, and overall efficiency are identified and computed. On the experimental side, tube performance is evaluated first without the MDC. Next the spent beam is analyzed for symmetry, circularity, and velocity spread, which permits determination of the size of the collector apertures. Finally, the MDC is attached and its performance optimized and evaluated.

The three-dimensional theory for ideal tubes with symmetric, circular, and optimally refocused beams predicts MDC efficiencies at midband of 89 percent for a two-stage MDC and 84 percent for a four-stage MDC. These calculations include an approximate computation of efficiency loss due to secondary electron emission for copper collecting surfaces.

Experimental results to date have yielded MDC efficiencies of 81 to 83 percent over the full octave bandwidth for a two-stage collector and 83.6 to 85 percent for a four-stage collector using soot as the electrode coating to suppress secondary electrons.

STAR Cat. 33

INTRODUCTION

The residual energy left in spent electron beams that exit from microwave tubes represents an unnecessary loss in efficiency and poses a heat dissipation problem. The reduction of these losses is mandatory in modern space communication systems, military countermeasure systems, and other high-power applications. This need led to the development of a number of novel depressed collectors (refs. 1 to 3) and spent-beam refocusing methods (ref. 4). The NASA-developed collector was successfully demonstrated in 1973 in conjunction with a 12-GHz, permanent-periodic-magnet focused TWT developed for the communications Technology Satellite (CTS) by Litton Industries (ref. 5). In this application an experimental TWT achieved an overall efficiency of 56 percent with a nine-stage MDC working at 81 percent collector efficiency. Using the technology developed for the CTS project has enabled the collectors that have been designed for the present application to be smaller and have fewer parts without sacrificing efficiency. This has been accomplished even though the military tubes have much larger beam perveance and bandwidth.

At this point it seems appropriate to discuss the concepts for evaluating and comparing collector performances, especially in view of the growing number of reported results. Many investigators use only estimated values for circuit losses, intercepted power, and power caused by backstreaming electrons (if any at all) to compute the input power into the collector. Collector efficiency cannot be determined accurately without measuring these quantities.

The performance of a collector should not be judged only by its efficiency η_c but rather in conjunction with many other factors. The η_c depends critically on the basic tube efficiency and also on the type of the tube.

Large beam size, large perveance, and large basic efficiencies reduce η_c, while a large number of plates and a large collector geometry tend to increase η_c if other factors are left unchanged. These considerations led to a general conclusion that it is easier to achieve higher η_c for small (or smaller) power tubes than for tubes with large power outputs.

The number of electrodes affects η_c, but the effect depends critically not only on the basic tube efficiency but also heavily on the shape of the spent-beam energy curve. Therefore, it is more difficult to develop equally efficient collectors for klystrons than for TWT's although both may have similar basic efficiencies. All these factors should be considered in the design when not only an efficient but also a simple and small collector is required.

In this report, the design philosophy underlying NASA-type collectors and the experimental methods and performance results are discussed and evaluated.

DESIGN CRITERIA FOR THE MULTISTAGE DEPRESSED COLLECTOR

Every microwave tube produces an electron beam at its output that is characteristic of the design, type of focusing, and level of performance of the amplifier. For this reason, an optimum depressed collector design must be arrived at on an individual basis such that the number, potentials, and location of the collector stages as well as the aperture size best "match" the spent beam. This matching can be improved by subjecting the beam to refocusing, the latter also being designed for the individual requirement.

It can be shown (ref. 3) that in all axisymmetric, magnetic-field-free MDC's, the highest efficiencies are obtained only when the collector size and the lengths of all trajectories are large compared with beam size; that is, the beam approximates a point source at the input. This result follows because an electrostatic MDC must convert a small part of the injection energy into radial deflection to accomplish sorting into energy classes and this energy cannot be recovered.

Figure 1 shows a sample of computed electron trajectories plus one test electron. The electron was injected with a (representative) angle of $+3^{\circ}$ and a total kinetic energy of $+0.5\ V_o$. At the apex it approaches an equipotential line at $-0.485\ V_o$; thus, it could be, in principle, collected with 97 percent efficiency. If more deflection is applied, the beam spreads farther away from the axis, electron penetration is less deep, and the sorting efficiency is lower. Occasionally it is, however, necessary to increase the amount of dispersion in order to improve the MDC efficiency. This is particularly true for a spent beam with a substantial fraction of electrons that have small negative angles (approx -1°) because these electrons tend to fall into the injection hole or onto the undepressed electrode.

The best aperture size is the smallest opening through which almost all trajectories can penetrate. Figure 2 shows extremely small negative angles, and figure 3 shows large positive angles as the other side of extreme entrance conditions. Thus, the aperture size is determined by the largest radial velocity components in the beam, which, in turn, depend partially on the quality of refocusing. It has been shown (ref. 6) that the standard deviation of the radial

velocity spread can be reduced in this application by a factor of 2 to 3 when an optimum expansion in the refocuser is applied. Simultaneously, the space charge is diluted such as to become unimportant in the collector region. Thus, two important functions can be carried out in a simple static arrangement with no power consumption.

Figure 4 shows schematically the principle of magnetic refocusing, which was originated and developed at Lewis (ref. 4). As the beam expands in a decaying magnetic field (possibly a permanent magnet field with reversal), transverse velocities are transformed in axial motion. This arrangement is very different conceptually from applying a simple magnetic lens to the end of the tube. Such an additional magnetic lens squeezes the spreading spent beam and permits smaller entrance angle conditions into the collector. It does, however, increase the radial velocity spread, which leads to larger losses in collector efficiency than are achievable with optimum refocusing.

It has been found at Lewis that when actual spent-beam trajectories are considered, the best refocusing field configuration is between 1 and 3 cyclotron wavelengths long in the decaying region and approximately 1/2 cyclotron wavelength long in the plateau region. Referring to figure 4, the first wavelength is defined in terms of the main focusing field (rms for PPM), and the second cyclotron wavelength is defined in terms of the plateau field. Average beam velocity is used in both cases. It is shown later in the text that a good refocusing design improves collector efficiencies by about 10 percentage points for tubes with electronic efficiency $\eta_c \leq 0.2$. The benefits of a good beam refocuser are also larger for higher perveance (space charge) beams than for lower perveance beams.

ROLE OF SECONDARY ELECTRONS IN MULTISTAGE-DEPRESSED-COLLECTOR OPERATIONS

To understand the phenomena created by the secondary emission processes, we shall review the typical energy spectrum of secondary electrons impinging on a pure metal structure, such as copper or molybdenum (ref. 7). For most pure metals, at perpendicular incidence and an impact energy of hundreds of volts, the secondary yield is 1.0 to 1.5. More than 90 percent of the secondary electrons come off the surface at energies peaking around 10 eV. There is, however, a second small peak in the secondary spectrum that occurs at the impact

energy of the primary electrons ("elastic reflection"). The yield between these two peaks is small but not zero. In all instances, the yield increases significantly, with the angle of primary incidence becoming more oblique. The contamination of the metal with oxide films also raises the yield by a significant factor as compared with a chemically pure metal. Since it is very difficult to obtain oxygen-free surfaces even in ultra high vacua, we should expect the secondary electron yield in practical cases to be higher than in extremely pure metals.

A study of the trajectory plots in figures 1 to 3 shows also that most primary electrons impact on the "upper" side (i.e., on the side away from the tube) but with angles 45° to 75° from normal incidence. We should, therefore, expect a secondary electron yield of about 2 because of this oblique impact. Now, the low-energy secondary electrons freed on "upper" sides will probably be suppressed by the strong negative field of the collector. A few percent of higher energy secondary electrons and reflected primary electrons have, however, the ability to escape from the plates and stream back to less depressed electrodes or to the body potential. The secondary electrons resulting from the small percentage of primary electrons impinging on the "lower" sides and the cone will certainly stream backward, although in most cases only to the next collector plate. Therefore, secondary electron emission results in some efficiency loss. A number of low-secondary-yield materials promise excellent suppressing characteristics for application in practical MDC's.

DESCRIPTION AND REVIEW OF ANALYTICAL RESULTS

The TWT/MDC performance is analyzed in three steps. For the computation of three-dimensional, axisymmetric trajectories in the TWT, our modification of a computer program developed by H. Detweiler (ref. 8) of the University of Michigan is used. The modification includes the addition of losses, severs, and drift regions. Thirty-two trajectories per cycle are being tracked. At the tube output, $\dot{z}$, $\dot{r}$, $r\dot{\phi}$, and r for each of the 32 charges are printed out, in addition to radiofrequency (rf) voltage, rf efficiency, integrated circuit losses, and interception. The output trajectories from the TWT are fed as input vectors into the spent-beam refocusing section and then into the MDC. For computations in the latter sections, computer programs developed at the Lewis Research Center are used. These three-dimensional programs take into account the space charge and magnetic fields. Computer samples of the output at the end of the TWT and at

the end of the spent-beam refocusing section (computed in part by N. Stankiewicz of Lewis) are given in table 1. As a function of trajectories 1 to 32, the vertical columns indicate the radius at TWT output, RI, in units of helix radius and both the axial velocity VI and the angle AI with respect to the tube axis. Subsequent columns refer to the end of the refocusing section (identical to the entrance into the MDC) and indicate the radius RF, the velocity VF, the angle AF, and the total kinetic energy in eV/eV_o. A few interesting and important conclusions can be made from reviewing the results of table 1, which are listed in the two rows labeled "average" and "standard deviation" and the columns AI and AF: We note that there are no negative angles at the collector input and that the average radius RF is more than twice RI, while the standard deviation of the final angle σ AF (collector input) is less than one-half that of the input angle σ AI into the refocuser. These values clearly demonstrate the beneficial effects of spent-beam refocusing. The space charge is reduced by a factor of 4 and the standard deviation of radial velocities (final angles, AF) is decreased by more than a factor of 2.5. The absence of negative input angles into the MDC, especially those in the range between -1.5^o and 0^o, is of particular significance because these trajectories will most likely return into the beam hole or land on the undepressed electrode.

A few comments are necessary concerning the experimental TWT with which the reported MDC experiments were conducted. Although the tube performed satisfactorily in most aspects, it exhibited unexpectedly high circuit losses, equivalent to more than 1 decibel per inch. This loss may be caused by some deviation from intended design or by some damage during or after construction, possibly in the attenuator. For this reason, it was not feasible to achieve a full correlation between computation and measurements in the TWT performance. Therefore, computations were carried out to produce the same total power conversion (rf plus losses) by using measured gain and interception. For the expected circuit losses (about 0.5 to 0.6 dB/in.), the vector velocity distribution would be somewhat different. However, the computer output sample (table 1) is certainly indicative of the potential of applying the developed analytical tools to efficiency optimization.

The 32 trajectories are injected as vectors (RF, VF, AF) into the depressed collector, which has a predetermined internal electric field distribution. Figure 5 shows the 32 trajectories. Figure 5(a) shows the trajectories with the smallest injection angles, figure 5(f) those with the largest injection angles. After the selection of electrode location and aperture size, the collector efficiency

was determined by summing the kinetic energy converted into potential energy at the landing on one of the electrodes and dividing it by the total kinetic energy at injection. For the sample with four electrodes between ground and cathode, the computed collector efficiency was 84 percent. For two stages (plus the cone with spike at cathode potential), this efficiency was 80 percent. The secondary yield was assumed to be unity for impacts on the "lower" sides and on the cone and to be zero for impacts on the "upper" sides. Reflected primaries were ignored entirely. It is clear that these assumptions are highly optimistic in view of the experimental evidence and theoretical evaluations.

The effectiveness of refocusing to improve the MDC performance even for tubes of a relatively low conversion efficiency, $\eta_e < 0.2$, was demonstrated convincingly by first injecting into the very same MDC the unrefocused beam parameters (VI, AI, RI) of table 1 and computing the MDC efficiency with identical assumptions as before. Efficiency decreased to 75 percent (from 84 percent). These analyses were carried out for an MDC with a gross height of 7.6 centimeters (3 in.) and a diameter of 5.1 centimeters (2 in.). The distance from the injection hole to the apex of the cone is 6 centimeters (2.36 in.), and the spike is typically less than 1 centimeter (0.4 in.) long for optimum efficiency.

ANALYSIS OF COLLECTOR INEFFICIENCY

Direct three-dimensional computation of actual electron trajectories permits a determination of collector inefficiency as well as an analysis of its sources. Figure 6 identifies six sources. The first four apply to a symmetric, circular, optimally refocused beam. When the beam is asymmetric and/or noncircular, the optimum design is compromised by the necessity of creating larger apertures and a possible impingement on "low" sides.

The effect of a finite number of electrodes on collector inefficiency depends strongly on the electronic efficiency of the tube and on the magnitude and shape of the energy distribution curve of the spent beam. The values given in figure 6 are valid for the case discussed in this report. Even with good refocusing there is still some loss due to residual radial velocity spread (listed as item 3). With no refocusing at all, an additional loss of 9 percent would occur. At high frequencies and/or high perveances, losses due to space-charge effects would arise that are virtually nonexistent with effective refocusing. In item 4, the experimentally determined effect of secondaries for the MDC design reported herein has been

listed. The values are lower bounds since the secondary suppression coating used (soot) gives far from perfect suppression.

Finally, it is important to see quantitatively how the collector efficiency η_c affects the overall efficiency η_{ov}, which is the only efficiency of interest to the system designer. In figure 7(a), η_{ov} is presented as a function of η_c with the electronic efficiency η_e of the tube alone as parameter for the case of no interception, no second harmonic, and zero circuit losses. Figure 7(b) shows the effect of circuit losses for an η_e of 0.15 obtained by applying formula 4 of reference 3. It can be seen that for tubes with low electronic efficiency, η_{ov} rises very rapidly in the neighborhood of $\eta_c \gtrapprox 0.8$. It is useful, therefore, to increase η_c as much as possible, as long as it can be accomplished without sacrificing the simplicity and size of the collector.

TRAVELING WAVE TUBE

The MEC TWT M5897C as modified for use in this program and its performance characteristics are shown in figure 8. A refocusing system consisting of two coils has been added. The TWT is mounted on a 25.4-centimeter (10-in.) UHV flange that houses a unique ultra-high-vacuum (UHV) valve (ref. 9). During MDC installation and changes, the valve can be closed and the TWT kept under vacuum, facilitating startup and enabling many collector changes without cathode activation problems. However, the valve's small size (an i.d. of 0.625 cm (0.250 in.)) and location (past the output pole piece of the refocusing section) impose limitations on beam expansion and refocusing range. Originally, the TWT had an undepressed collector mounted on a matching 25-centimeter (10-in.) UHV flange. An identical matchting flange exists on the vacuum system used for subsequent tests.

EXPERIMENTAL PROGRAM

The experimental program consists of a bench test, a beam test, and MDC tests.

Bench Test

The purpose of the bench test is to document the performance of the TWT with an undepressed spent-beam collector so that TWT performance changes, if any, due to the MDC can be determined and so that accurate MDC efficiency measurements can later be made. The power flow diagram for the TWT with an undepressed thermally isolated collector is shown in figure 9(a). The rf load, TWT body, and collector are all thermally isolated and water cooled. Thermal power to each is measured by a combination of flowmeter and thermopile. Part of the I^2R losses in the air-cooled refocusing coils shows up in the body cooling loop, but this small contribution is subtracted by an offset technique. Since the collector is undepressed, the power returned to the TWT by any backstreaming electrons is negligible. The measured P_{body} is, therefore, the sum of the total rf losses in the TWT and the interception losses. To identify the contribution of each to P_{body}, an assumption must be made about the average energy of the intercepted electrons.

The rf setup is shown in figure 10. The sum of rf power at the fundamental and second harmonic frequencies is dissipated by the rf load.

Data from all tests are obtained with an automated data acquisition system. A steady state is established and 100 scans are taken on all measurements and averaged to improve accuracy.

Beam Test

The purpose of the beam test is to evaluate the effectiveness of the refocusing system and to obtain information needed to guide in the selection of MDC aperture sizes and MDC stage voltages. The beam test consists of the following:

(1) Measurement of the angular distribution of spent-beam power with a segmented axisymmetric collector/calorimeter

(2) Measurement of the range of electron energies with a retarding electric field energy analyzer

(3) Evaluation of the beam circularity and symmetry by visual observation of the spent-beam impinging on the collector/calorimeter face

The beam test setup is shown in figure 11. The undepressed collector has been removed, and the spent beam is collected by an axisymmetric segmented-beam collector/calorimeter consisting of a circular center segment and four

concentric rings. These water-cooled semgnets are thermally and electrically isolated from each other, and the current collected by and the power dissipated on each segment are measured. The electron energy analyzer samples only a small fraction of the beam on (and near) the axis.

The beam striking the collector/calorimeter face generates sufficient luminosity to be visible through the viewport. Beam circularity and symmetry are evaluated visually. The beam tests are performed in a vacuum of 10^{-9} to 10^{-10} torr as measured with an ionization gage in the UHV chamber.

The beam test gives only limited information. The spent beam looks like a point source to this collector/calorimeter, and it cannot distinguish positive and negative (toward axis) electron angles. Only total power to each segment is measured; no information is obtained on the specific contributions of the various electron energy classes to this total. Consequently, virtually no information is obtained on the amount and distribution of dispersion required in the MDC. Considerable judgment must be exercised in the selections of the individual MDC stage apertures based on beam test results.

Multistage-Depressed-Collector Tests

During these tests, various MDC's are added to the TWT and the performance is evaluated. The MDC test setup is shown in figure 12. The MDC is mounted directly on the UHV flange which houses the TWT/vacuum valve. Each MDC plate is thermally and electrically isolated and is water cooled. The spent-beam power recovered by each MDC plate as well as the thermal power dissipated on each plate are measured. A vacuum feedthrough drives a variable-length spike. Since the refocusing coils and pole pieces are external to the vacuum, they can be manipulated while the TWT is operating.

A typical experimental collector is shown in figure 8. This particular fully demountable mechanical design was chosen for experimental convenience and permitted rapid and easy MDC changes. Water cooling (and calorimetry) of each plate separately was chosen for diagnostic purposes and to provide information for the eventual thermal design of a conduction-cooled MDC.

The internal (active) volume of the MDC is that within the inner diameter of the cooling lines (i.d. of 5.1 cm (2.00 in.)). The electrode geometries within this volume are critical to the MDC performance, but the electrode support structure outside is not. Extensive thermal and mechanical design changes will have to be made to adapt these MDC's to practical TWT's.

The power flow diagram for the TWT with an MDC is shown in figure 9(b). Part of the beam power appears as measured rf output power, and part is dissipated on the TWT body as the sum of rf losses in the TWT and intercepted beam power in the forward direction. The rest enters the MDC. Part of the power into the collector is recovered as electric power, and part is dissipated as thermal power on the MDC plates. Also, with an MDC, the possibility exists of backstreaming electrons returning significant power to the TWT body. This contribution to P_{body} can be evaluated only by comparing these results with the previously obtained bench test results since the TWT body calorimeter cannot distinguish true interception of the forward beam from backstreaming electrons collected on the TWT body. Consequently, accurate MDC efficiencies, defined as $P_{recovered}/P_{coll\ in}$ can be determined only by performing both the MDC test and the bench test. The power into the collector can then be determined as $(V_K I_K - P_0 - P_{body,\ bench\ test})$. These considerations apply when TWT performance is sufficiently repeatable from test to test.

During an MDC test, the following are varied to optimize performance:

(1) Individual collector stage voltages

(2) Individual refocusing coil currents

(3) Refocusing coil/pole piece locations

(4) Variable spike length

A novel data acquisition system is used to optimize MDC performance under various conditions (frequency, level of saturation, etc.). This system provides an analog real-time readout of $P_{recovered}$ as any of the preceding are varied. Maximizing $P_{recovered}$ under a given operating condition is identical to maximizing the true MDC efficiency at this condition. The automated data acquisition system is used for actual data taking.

The MDC tests are performed in vacuums of 10^{-9} to 10^{-10} torr. The planned MDC geometric variables include MDC size, number of plates, collector plate aperture size, and collector plate shape.

EXPERIMENTAL RESULTS

To date, the bench test, several beam bests, and 11 MDC tests have been completed.

Bench Test Results

The rf output power and rf losses in the TWT as a function of frequency are shown in figure 13. The rf losses of this TWT are much higher than cold helix measurements predict. (The circuit efficiency at some frequencies is as low as 67 percent.) It is doubtful if these high rf losses are typical of this class of TWT's. If so, they would severely limit the improvement obtainable in the overall TWT efficiency by the addition of an MDC.

In computing the circuit losses it has been assumed that the average energy of the intercepted electrons is eV_k. The range of alternative assumptions that could be made modifies the results only slightly since the interception of this TWT averages less than 1 percent without depression and since the electronic efficiency is also relatively low ($\eta_e < 0.18$), such that little energy is extracted from the beam.

The indicated rf losses are believed to be lower limits since the 1-percent-or-better total energy balance gave less total thermal power than the total electrical input power in all cases. The probable cause is the reduction of the fraction of I^2R losses in the refocusing coils that are conducted to the TWT body, as it gets hot under operating conditions.

Approximately twice the analytically predicted magnetic field was needed from the second refocusing coil to prevent excessive interception on the refocusing tunnel.

Beam Best Results

The angular power distribution across the frequency band at saturation was as follows:

(1) -3° to $+3^\circ$ for 56 to 74 percent of P_{coll} in

(2) $-4\frac{1}{3}^\circ$ to $+4\frac{1}{3}^\circ$ for 82 to 90 percent of P_{coll} in

(3) $-6\frac{2}{3}^\circ$ to $+6\frac{2}{3}^\circ$ for 92 to 96 percent of P_{coll} in

(4) $-9\frac{1}{2}^\circ$ to $+9\frac{1}{2}^\circ$ for 97 to 99 percent of P_{coll} in

The spent beam was both noncircular and unsymmetric. The beam image is shown in figure 14. Evaluation shows that the up to 8 percent and 3 percent of spent-beam power that appear at angles greater than $6\frac{2}{3}^\circ$ and $9\frac{1}{2}^\circ$, respectively, are due largely to beam asymmetry. Energy analyzer results showed an electron energy range of 6.2 to 11.9 keV, very close to analytical predictions.

Multistage-Depressed-Collector Test Results

To date, all tests have been conducted with a 7.6-centimeter (3-in.) high by 5.1-centimeter (2-in.) diameter (internal volume) collector consisting of six collecting plates, which include a cone-shaped plate at cathode potential and a plate at TWT body potential. The number of stages is defined as the number of individual voltages, other than V_k and TWT body potential, required to operate the MDC. Experiments were made in four-stage and two-stage (obtained by electrically connecting the intermediate plates into two sets) configurations.

Two types of optimizations were stressed: optimization of MDC efficiency at 4.8-GHz (lower frequency edge) saturated output and at the maximum prime power point (near midband). However, with performance optimized at the maximum prime power point, excessive interception resulted at the low band edge at times. Since substantially lower than normal currents were required in the first refocusing coil to produce this optimum, it is believed that true interception of the forward-moving beam resulted during operation at the low band edge. Current in this coil was increased slightly and a few tenths of 1 percent of MDC efficiency was sacrificed to enable operation across the entire band.

The MDC design for the initial MDC tests was based on analytical results of the refocusing study. Since all electron angles were positive, minimal additional dispersion was introduced by the MDC. This design is shown in figure 15. Experimental results are shown in table 2. The following conclusions were reached from the initial MDC tests:

(1) Experimental results deviate from analytical predictions.

(a) MDC efficiencies are significantly below the analytical predictions. Backstream electrons that are returned to the TWT and to the undepressed MDC plate are the cause of much of the reduced MDC efficiency.

(b) The spent beam seems to differ radically from that predicted by the refocusing system analysis. The much larger than predicted magnetic field that is needed from the second refocusing coil to prevent excessive interception might be producing a large number of electrons with negative injection angles. (This restriction can be eliminated by enlarging the refocusing tunnel and UHV valve aperture size.)

(c) The spent beam seems to exhibit two peaks in the electron velocity density function rather than the somewhat uniform distribution that was predicted.

(d) The refocusing analysis must be refined to obtain better agreement with measurements.

(2) MDC efficiency is high for fast electrons.

(3) MDC design provides insufficient dispersion for any slow electrons with negative injection angles.

(4) This spent beam is far from the ideal point source for this small MDC. This is particularly significant if a substantial number of electrons have negative injection angles.

During the course of these tests, the TWT UHV valve failed. On all subsequent MDC changes, the TWT had to be backfilled with gaseous nitrogen and subsequently rf processed under pulsed conditions. However, this turned out to be less of a problem than anticipated. Only a few hours of pulsed operation were needed before continuous-wave operation could be achieved. Also, the TWT performance was found to have changed at one point during these tests. In the range 5.6- to 7.2-GHz, P_0 was lower and P_{body} was higher. At some higher frequencies, P_0 was slightly higher and P_{body} lower. After this, most of the data were taken at the band edges and at the maximum rf output power point at 8.0 and/or 8.4 GHz. In calculating the MDC efficiency, the measured P_{body} (not bench-test P_{body}) was used, since the TWT performance had changed.

A series of changes were made in the MDC design to adapt it to the spent-beam characteristics of this particular TWT. Five different MDC designs were experimentally produced. Each design involved a series of changes and evolved from analyzing the results from the previous test. Four of the designs led to improved MDC efficiency, while one produced slightly lower MDC efficiency. The design that finally evolved is a complex one with a highly nonuniform electric field distribution in the MDC and consequent lens effects. Electrolytic tank results showed regions of convergence as well as divergence. These lens effects were experimentally exploited to maximize the MDC efficiency. The sequence of changes and experimental results are detailed here.

The initial MDC modifications (MDC 1WX1) were the following:

(1) First (lowest) depressed stage
   (a) Angle increased from 11° to 15° 40'
   (b) Aperture decreased slightly

(2) Second depressed stage: angle increased from 12° 12' to 17°

(3) Defocusing electrode added

(4) "Baffle" system added to limit both electron penetration beyond the 5.1-centimeter (2-in.) diameter and possible escape out the relatively open sides of the MDC

MDC 1WX1 is shown in figure 16. The results are shown in table 3. The number of backstreaming electrons collected on the TWT body and on the undepressed plate was reduced but remained substantial. MDC efficiency was improved approximately 3 percentage points for the four-stage condiguration and approximately 5 percentage points for the two-stage configuration.

The defocusing electrode was electrically isolated and its potential could be varied to optimized MDC efficiency. Best results were obtained with this electrode at TWT body potential. A substantial efficiency loss due to elastically and inelastically scattered primary electrons from all collecting surfaces was hypothesized. The following MDC modifications were made:

(1) First depressed stage
   (a) Angle increased from 15^{o} 40' to 20^{o}
   (b) Aperture decreased substantially
(2) Second defocusing electrode added
(3) First defocusing electrode relocated
(4) Secondary suppression coating (soot) added to all collecting surfaces
(5) MDC relocated closer to TWT (This effectively increased all plate apertures slightly.)

MDC 1WX3 is shown in figure 17. The results with MDC 1WX3 are shown in table 4. With the same MDC voltages used in the previous test, the number of backstreaming electrons was reduced very substantially. All MDC stages could be significantly more depressed without an excessive increase in the number of backstreaming electrons, thus leading to additional MDC efficiency improvement. The total improvemen in MDC efficiency was 5 to 6 percentage points for both the two-stage and four-stage configurations.

During the course of this MDC test, one of the refocusing coils failed. Since the highest MDC efficiencies had been obtained at one limit of the variability of the refocusing system, it was decided to modify the relative lengths of the refocusing coils. A small but not general efficiency improvement was obtained. The results are shown in tables 5 to 8. Table 5 shows TWT and MDC performance optimized at 4.8 GHz (saturation). Table 6 shows TWT and two-stage MDC performance optimized at the maximum prime power point. Under these conditions, the MDC efficiency improvement during operation below saturation is limited. However, by increasing the depression of the second stage so as to sacrifice 0.8 percentage point of MDC efficiency at the optimization point, a substantial gain in MDC efficiency can be realized at operating levels below saturation. This is shown in table 7. Table 8 shows TWT and four-stage MDC performance under slightly less compromised conditions.

In general, two-stage MDC efficiencies of 78 to 81.5 percent were obtained at saturation. Four-stage MDC efficiencies ranged from 80.4 to 82.0 percent at saturation. During a subsequent MDC test, it was established that the MDC efficiency improvement due to the secondary suppression coating (soot) alone was 2.7 to 4.7 percentage points for both the two- and four-stage configurations, with the largest improvement occurring at band edges.

The overall efficiency based on the output power at the fundamental frequency is limited by the large amount of second harmonic power generated at the low band edge and by the excessive TWT rf losses at the higher frequencies. The following modifications were made:

(1) Second depressed stage: angle increased from 17^{o} to 20^{o}

(2) Third defocusing electrode added (at the potential of the second depressed stage)

(3) Apertures in the third and fourth depressed stages enlarged

(4) Soot coating more carefully and completely applied

MDC 1WX4 is shown in figure 18. The results with MDC 1WX4 are shown in tables 9 to 12. Tables 9 and 10 show two-stage MDC and TWT performance optimized at 8.4 and 4.8 GHz, respectively. Tables 11 and 12 show four-stage MDC and TWT performance optimized at 8.4 and 4.8 GHz, respectively. A significant improvement was obtained in both MDC and TWT overall efficiency. Minimum MDC efficiencies were 80 and 82 percent for the two- and four-stage configurations, respectively.

Next the apertures in the four depressed plates were enlarged. MDC 1WX5 is shown in figure 19. The two-stage MDC performance at saturated power output is shown in table 13 for the two optimizations. The MDC/TWT performance at and below saturation is shown in table 14. The optimization for 8.4 GHz produced two-stage MDC and overall efficiencies of 82.1 and 39.0 percent, respectively, and a minimum collector efficiency of 81 percent.

The four-stage MDC performance at saturation is shown in table 15 for various optimizations. The MDC and TWT performance at and below saturation is shown in table 16. The optimization for 8.4 GHz produced MDC and overall efficiencies of 84.2 and 41.6 percent, respectively. Alternately, the MDC could be optimized to produce a minimum collector efficiency of 83.6 percent.

As already noted, the actual (not bench test) body power was used in computing MDC efficiency since the TWT performance had changed. This did not result in significantly exaggerated MDC efficiencies because almost all of the backstreaming electrons are collected on the air-cooled UHV valve tunnel or

refocusing section tunnel and do not contribute to the measured body power. Therefore, backstreaming produced by the MDC is charged against it. However, for any contribution to measured body power due to backstreaming electrons, the MDC efficiency would have to be decreased by 1 percentage point per 35 W. For purposes of comparison between the bench test and the results of MDC 1WX5 at 4.8 GHz, the body power had increased by 24 to 48 W, at 8.4 GHz it was essentially unchanged, and at 9.6 GHz it had decreased slightly.

The improvement in the overall efficiency due to the MDC's was severely limited by the excessive TWT rf losses at the higher frequencies and by the large amount of harmonic power at the low band edge.

Details of the MDC geometries are given in appendix A. The refocusing system is described in appendix B. Some performance details for MDC 1WX5 are given in appendix C.

CONCLUDING REMARKS

Experimental evaluation of a small two-stage depressed collector indicated octave bandwidth collector efficiencies between 81 and 83 percent, which closely approaches the analytically predicted performance in conjunction with a high-performance TWT of 330- to 550-W power output and 0.5 microperveance. Addition of two more stages produced only a few percentage point gain in collector efficiency. Secondary electron emission can lead to significant MDC efficiency losses. The absence of secondary suppression coating on the electrode surfaces reduced collector efficiency by about 2.7 to 4.7 percentage points. Further small improvements in collector efficiency can probably be obtained by optimizing the spent-beam refocuser. Assuming normal circuit losses (circuit efficiencies ≥ 0.85) and a similar basic efficiency, overall tube efficiencies in excess of 40 percent should be possible across most of the octave bandwidth.

Lewis Research Center,
National Aeronautics and Space Administration,
Cleveland, Ohio, August 6, 1976.

REFERENCES

1. Neugebauer, Wendell; and Mihran, Theodore: A Ten-Stage Electrostatic Depressed Collector for Improving Klyston Efficiency. IEEE Trans. on Education, vol. ED-19, no. 1, Jan. 1972, pp. 111-121.

2. Okoshi, Lakanori; Chiu, Eng-Beng; and Matsuki, Sadov: The Tilted Electric Field Soft-Landing Collector and its Application to a Traveling-Wave Tube. IEEE Trans. Education, vol. ED-19, no. 1, Jan. 1972, pp. 104-110.

3. Kosmahl, Henry G.: A Novel, Axisymmetric, Electrostatic Collector for Linear Beam Microwave Tubes. NASA TN D-6093, 1971.

4. Kosmahl, H.: An Electron Beam Controller. U.S. Patent 3,764,850, 1973.

5. Kosmahl, Henry; McNary, B. D.; and Sauseng, Otto: High Efficiency, 200-Watt, 12-Gigahertz Traveling-Wave Tube. NASA TN D-7709, 1974.

6. Stankiewicz, N.: Evaluation of Magnetic Refocusing in Linear-Beam Microwave Tubes. NASA TN D-7660, 1974.

7. Beck, Arnold H., ed.: Handbook of Vacuum Physics. Vol. 2; Physical Electronics. Pergamon Press, 1966.

8. Detweiler, H. K.: Characteristics of Magnetically Focused Large Signal TWT Amplifier. University of Michigan, (RADC-TR-68-433; AD-842733), 1968.

9. Gilmour, A. S., Jr.: Study of Miniaturized UHV Gate Valves. Rome Air Develop. Center (Job Order No. 956731), 1975.

APPENDIX A

MDC GEOMETRY DETAILS

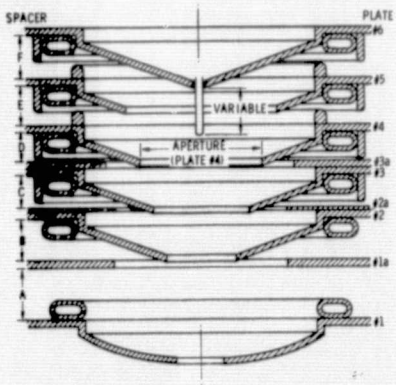

Plate number	Spacer	1W		1WX1		1WX3		1WX4		1WX5	
		Angle, deg									
1		(a)		(a)		(a)		(a)		(a)	
1A				0		0		0		0	
2		11^{o} 4'		15^{o} 40'		20^{o}		20^{o}		20^{o}	
2A						0		0		0	
3		12^{o} 20'		17^{o}		17^{o}		20^{o}		20^{o}	
3A								0		0	
4		14^{o} 24'		14^{o} 24'		14^{o} 24'		14^{o} 24'		14^{o} 24'	
5		17^{o}		17^{o}		17^{o}		17^{o}		17^{o}	
6		20^{o}		20^{o}		20^{o}		20^{o}		20^{o}	
		Aperture size									
		cm	in.	cm	in.	cm	in.	cm	in.	cm	in.
1		0.686	0.270	0.991	0.390	1.016	0.400	1.016	0.400	1.016	0.400
1A				3.810	1.50	3.810	1.50	3.810	1.50	3.810	1.50
2		1.887	.743	1.681	.662	1.461	.575	1.461	.575	1.524	.600
2A						3.810	1.50	3.810	1.50	3.810	1.50
3		2.220	.866	2.141	.843	2.141	.843	2.141	.843	2.337	.920
3A								4.064	1.60	4.064	1.60
4		2.527	995	2.527	.995	2.527	.995	2.692	1.060	2.794	1.100
5		2.845	1.12	2.845	1.12	3.845	1.12	3.239	1.275	3.683	1.450
6		.178	.070	.178	.070	.178	.070	.178	.070	.178	.070
		Thickness									
		cm	in.	cm	in.	cm	in.	cm	in.	cm	in.
	A			1.219	0.480	1.219	0.480	1.143 [b]	0.450	1.143	0.450
	B			.889	.350	.880	.350	.813	.320	.813	.320
	C			.813	.320	.550	.260	.660	.260	.550	.260
	D			.841	.331	.841	.331	.686	.270	.686	.270
	E			.884	.348	.884	.348	.884	.348	.884	.348
	F			.897	.353	.897	.353	.897	.353	.897	.353
1		0.152	0.060	.152	.060	.152	.060	.152	.060	1.52	.060
1A					.030		.030	.152	.060	.152	.060
2		.152	.060	.152	.060	.152	.060	.152	.060	.152	.060
2A						.076	.030	.076	.030	.076	.030
3		.152	.060	.152	.060	.152	.060	.152	.060	.152	.060
3A								.152	.060	.152	.060
4		.152	.060	.152	.060	.152	.060	.152	.060	.152	.060
5		.152	.060	.152	.060	.152	.060	.152	.060	.152	.060
6		.152	.060	.152	.050	.152	.060	.152	.060	.152	.060

[a] Plate 1 is curved with 6-cm (2.332-in.) spherical radius.

[b] Copper spacers (A) were used with MDC 1WX4 to electrically connect plates 1 and 1A. Otherwise, the plates are connected electrically and plate 1 is always grounded.

APPENDIX B

REFOCUSING SYSTEM

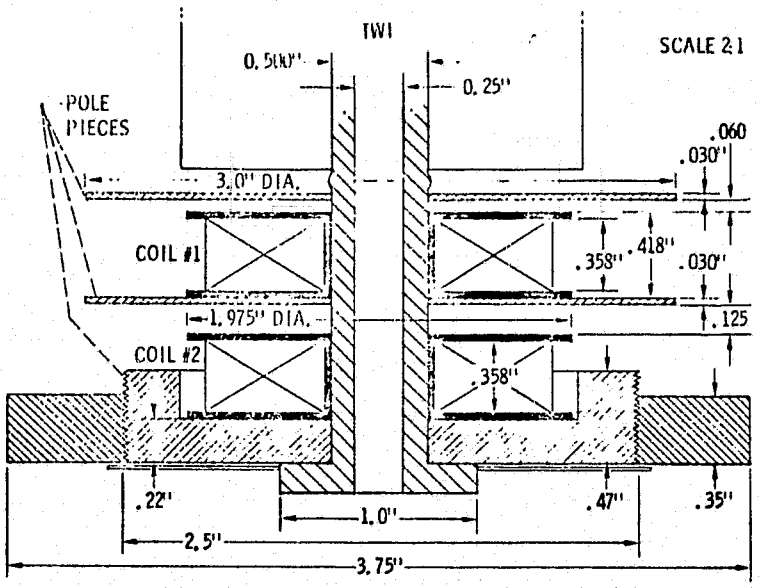

FOCUSING COILS AND DIMENSIONS - TYPICAL ARRANGEMENT

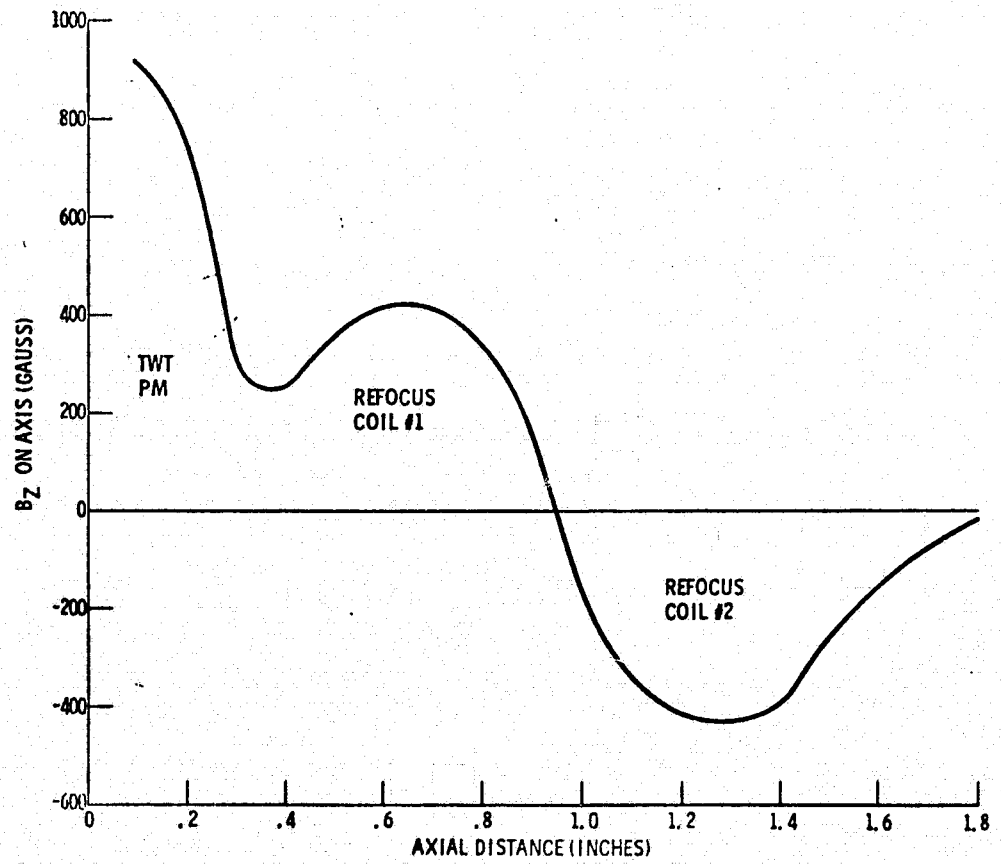

Typical refocusing field profile B_Z on axis vs. Z.

APPENDIX C

DETAILS OF MULTISTAGE-DEPRESSED-COLLECTOR PERFORMANCE

Two-Stage Configuration

The performance details of MDC 1WX5 optimized at 8.4 GHz (saturation) are given for frequencies of 4.8, 8.4, and 9.6 GHz (saturation).

(1) Frequency, 4.8 GHz (saturation)

	Voltage, kV	Current, mA	Recovered power, W	Thermal power dissipated, W
Cathode	-9.44	429.5	----	----
Body	-----	25.9	----	167
Radiofrequency load	-----	-----	----	[a]396
Collector:				
1	0	18.2	0	122
2	-5.24	48.5	254	54
3	-5.24	97.5	511	151
4	-8.7	14.1	123	29
5	-8.7	216.0	1879	136
6	-9.44	7.9	75	58
Total		402.2	2842	550

[a] $P_{(Fund)} = 281$ W.

(2) Frequency, 8.4 GHz (saturation)

	Voltage, kV	Current, mA	Recovered power, W	Thermal power dissipated, W
Cathode	9.44	429.5	----	---
Body	-----	17.5	----	221
Radiofrequency load	-----	-----	----	515
Collector:				
1	0	13.5	0	87
2	-5.24	72.8	381	63
3	-5.24	140.2	735	164
4	-8.70	13.4	117	30
5	-8.70	157.9	1374	116
6	-9.44	13.5	127	48
Total		411.3	2734	508

(3) Frequency, 9.6 GHz (saturation)

	Voltage, kV	Current, mA	Recovered power, W	Thermal power dissipated, W
Cathode	0.45	429.5	----	---
Body	-----	16.3	----	200
Radiofrequency load	-----	-----	----	344
Collector:				
1	0	9.6	0	66
2	-5.25	48.9	257	46
3	-5.25	116.6	612	164
4	-8.72	14.9	130	34
5	-8.72	214.5	1870	144
6	-9.45	6.9	65	42
Total		411.4	2934	496

Four-Stage Configuration

The performance details of MDC 1WX5 at compromise optimization are given for frequencies of 4.8, 8.4, and 9.6 GHz (saturation).

(1) Frequency, 4.8 GHz (saturation)

	Voltage, kV	Current, mA	Recovered power, W	Thermal power dissipated, W
Cathode	-9.44	430.95	----	----
Body	-----	18.1	----	151
Radiofrequency load	-----	------	----	[a]409
Collector:				
1	0.0	11.1	0	71
2	-5.1	58.6	299	52
3	-5.3	95.2	505	110
4	-8.12	47.6	387	51
5	-8.86	188.6	1671	110
6	-9.44	9.2	87	55
Total		410.3	2949	449

[a] $P_{(Fund)} = 284$ W.

(2) Frequency, 8.4 GHz (saturation)

	Voltage, kV	Current, mA	Recovered power, W	Thermal power dissipated, W
Cathode	-9.45	430.95	----	---
Body	-----	13.0	----	218
Radiofrequency load	-----	------	----	516
Collector:				
1	0.0	10.7	0	70
2	-5.1	99.3	506	83
3	-5.3	110.3	585	133
4	-8.12	48.0	390	54
5	-8.86	131.7	1167	88
6	-9.45	16.0	151	55
Total		416.0	2799	483

(3) Frequency, 9.6 GHz (saturation)

	Voltage, kV	Current, mA	Recovered power, W	Thermal power dissipated, W
Cathode	9.45	431.44	----	---
Body	-----	10.5	----	201
Radiofrequency load	-----	-----	----	336
Collector:				
1	0.0	7.2	0	55
2	-5.1	61.5	314	58
3	-5.3	96.8	513	132
4	-8.13	55.8	454	58
5	-8.87	186.6	1655	108
6	-9.45	9.7	92	41
Total		417.6	3028	452

TABLE 1. - ELECTRON SPECTRUM BEFORE AND AFTER REFOCUSING

Trajectory	RI	VI	AI	RF	VF	AF
1	0.556E+00	0.771E+00	0.783E+01	0.600E+00	0.774E+00	0.197E+01
2	0.516E+00	0.796E+00	0.282E+01	0.971E+00	0.797E+00	0.395E+01
3	0.409E+00	0.801E+00	-0.312E+01	0.170E+01	0.802E+00	0.496E+01
4	0.554E+00	0.808E+00	-0.194E+01	0.152E+01	0.808E+00	0.582E+01
5	0.353E+00	0.809E+00	-0.526E+01	0.203E+01	0.812E+00	0.442E+01
6	0.551E+00	0.816E+00	0.630E+01	0.676E+00	0.818E+00	0.159E+01
7	0.454E+00	0.828E+00	0.104E+01	0.112E+01	0.828E+00	0.397E+01
8	0.205E+00	0.837E+00	0.370E+00	0.151E+01	0.839E+00	0.300E+01
9	0.541E+00	0.839E+00	0.291E+01	0.867E+00	0.840E+00	0.332E+01
10	0.445E+00	0.843E+00	0.267E+01	0.980E+00	0.845E+00	0.289E+01
11	0.672E+00	0.846E+00	0.585E+01	0.574E+00	0.847E+00	0.206E+01
12	0.335E+00	0.855E+00	-0.392E+01	0.183E+01	0.857E+00	0.471E+01
13	0.249E+00	0.859E+00	-0.199E+01	0.166E+01	0.861E+00	0.397E+01
14	0.328E+00	0.864E+00	0.140E+01	0.122E+01	0.866E+00	0.301E+01
15	0.744E+00	0.866E+00	0.445E+01	0.596E+00	0.866E+00	0.326E+01
16	0.381E+00	0.866E+00	0.247E+01	0.197E+01	0.868E+00	0.261E+01
17	0.164E+00	0.883E+00	0.124E+00	0.162E+01	0.886E+00	0.306E+01
18	0.550E+00	0.897E+00	0.399E+01	0.775E+00	0.899E+00	0.182E+01
19	0.266E+00	0.898E+00	0.395E+00	0.138E+01	0.900E+00	0.330E+01
20	0.271E+00	0.915E+00	0.452E+00	0.143E+01	0.916E+00	0.367E+01
21	0.322E+00	0.921E+00	0.104E+01	0.123E+01	0.922E+00	0.307E+01
22	0.392E+00	0.928E+00	-0.390E+01	0.175E+01	0.929E+00	0.519E+01
23	0.517E+00	0.932E+00	-0.994E+00	0.116E+01	0.932E+00	0.471E+01
24	0.418E+00	0.938E+00	-0.252E+01	0.145E+01	0.939E+00	0.497E+01
25	0.525E+00	0.952E+00	0.483E+01	0.873E+00	0.954E+00	0.806E+00
26	0.256E+00	0.954E+00	-0.905E+00	0.147E+01	0.955E+00	0.383E+01
27	0.334E+00	0.982E+00	0.883E+00	0.114E+01	0.893E+00	0.303E+01
28	0.574E+00	0.101E+01	0.245E+01	0.772E+00	0.101E+01	0.191E+01
29	0.350E+00	0.101E+01	0.542E+00	0.116E+01	0.101E+01	0.314E+01
30	0.569E+00	0.103E+01	0.282E+01	0.793E+00	0.103E+01	0.152E+01
31	0.559E+00	0.109E+01	0.304E+01	0.861E+00	0.109E+01	0.114E+01
32	0.563E+00	0.111E+01	0.232E+01	0.815E+00	0.111E+01	0.142E+01
Average =	0.435E+00	0.898E+00	0.111E+01	0.118E+01	0.900E+00	0.319E+01
Standard deviation =	0.139E+00	0.835E-01	0.307E+01	0.394E+00	0.832E-01	0.126E+01

TABLE 2. - RESULTS FOR MDC 1W

Optimization frequency, GHz	Frequency, GHz		
	4.8	8.0	9.6
	Collector efficiency, η_c, percent		
Two-stage configuration			
4.8 (saturation)	70	65	70
Four-stage configuration			
8.0 (saturation)	73.5	71.5	74.5

TABLE 3. - RESULTS FOR MDC 1WX1

Optimization frequency, GHz	Frequency, GHz		
	4.8	8.0	9.6
	Collector efficiency, η_c, percent		
Two-stage configuration			
4.8 (saturation) 8.0 (saturation)	75 73.6	70.5 73.8	75.3 75.3
Four-stage configuration			
8.0 (saturation)	74.8	74.5	75.7

TABLE 4. - RESULTS FOR MDC 1WX3 WITH SECONDARY ELECTRON SUPPRESSION

Optimization frequency, GHz	Frequency, GHz		
	4.8	8.0	9.6
	Collector efficiency, η_c, percent		
Two-stage configuration			
4.8 (saturation)	79.9	76.5	81.3
Each frequency (saturation)	79.9	78.2	81.7
Four-stage configuration			
Each frequency (saturation)	81.6	80.4	83.5

TABLE 5. - RESULTS FOR MDC 1WX3 WITH MODIFIED REFOCUSING SYSTEM AND SECONDARY ELECTRON SUPPRESSION - OPTIMIZED AT 4.8 GHz (SATURATION)

Frequency, GHz	Fundamental efficiency, percent		Collector efficiency, η_c, percent
	Without MDC	With MDC	
Two-stage configuration			
4.8	6.9	22.9	80.7
8.0	12.5	33.7	77
9.6	8.3	28.4	81.1
Four-stage configuration			
4.8	7	24	81.5
8.0	12.6	35	78.4
9.6	8.3	29.9	82.6

TABLE 6. - RESULTS FOR MDC 1WX3 WITH MODIFIED REFOCUSING SYSTEM AND SECONDARY ELECTRON SUPPRESSION - TWO-STAGE CONFIGURATION OPTIMIZED AT 8.4 GHz (SATURATION)

Frequency, GHz	Fundamental efficiency, percent	Collector efficiency, η_c, percent
4.8:		
Saturation	21.2	77.5
-3 dB	15.2	81.6
-6 dB	8.0	81.6
-9 dB	4.6	82.8
-12 dB	2.5	84.2
8.4:		
Saturation	36.0	78.9
-3 dB	24.4	80.8
-6 dB	13.9	81.4
-9 dB	7.6	81.6
-12 dB	4.5	83.4
9.6:		
Saturation	26.7	79.6
-3 dB	16.5	80.9
-6 dB	9.3	81.6
-9 dB	5.1	83.0
-12 dB	2.7	84.3
Direct-current beam	----	84.9

TABLE 7. - RESULTS FOR MDC 1WX3 WITH MODIFIED REFOCUSING SYSTEM AND SECONDARY ELECTRON SUPPRESSION - TWO-STAGE CONFIGURATION NEARLY OPTIMUM AT 8.4 GHz (SATURATION)

Frequency, GHz	Fundamental efficiency, percent	Collector efficiency, η_c, percent
4.8:		
Saturation	23.3	80.0
-3 dB	17.7	84.8
-6 dB	10.4	85.8
-9 dB	5.8	86.8
-12 dB	3.3	88.3
8.4:		
Saturation	34.2	78.1
-3 dB	25.2	83.1
-6 dB	15.8	84.6
-9 dB	9.0	85.3
-12 dB	5.5	87.3
9.6:		
Saturation	26.4	81.5
-3 dB	17.5	83.7
-6 dB	10.5	85.3
-9 dB	6.1	86.3
-12 dB	3.6	88.4
Direct-current beam	----	90.8

TABLE 8. - RESULTS FOR MDC 1WX3 WITH MODIFIED REFOCUSING SYSTEM AND SECONDARY ELECTRON SUPPRESSION - FOUR-STAGE CONFIGURATION NEARLY OPTIMUM AT 8.4 GHz (SATURATION)

Frequency, GHz	Fundamental efficiency, percent	Collector efficiency, η_c, percent
4.8:		
Saturation	23.4	80.7
-3 dB	16.3	84.8
-6 dB	9.7	84.9
-9 dB	5.3	85.7
-12 dB	3.0	86.9
8.4:		
Saturation	37.0	80.4
-3 dB	25.5	83.1
-6 dB	15.7	84.4
-9 dB	8.8	84.8
-12 dB	4.9	86.3
9.6:		
Saturation	27.4	82.0
-3 dB	17.3	83.5
-6 dB	10.1	84.8
-9 dB	5.1	85.4
-12 dB	3.3	87.0
Direct-current beam	----	88.3

TABLE 9. - RESULTS FOR MDC 1WX4 WITH MODIFIED REFOCUSING SYSTEM AND SECONDARY ELECTRON SUPPRESSION - TWO-STAGE CONFIGURATION OPTIMIZED AT 8.4 GHz (SATURATION)

Frequency, GHz	Fundamental efficiency, percent		Collector efficiency, η_c, percent
	Without MDC	With MDC	
4.8:			
Saturation	7.0	22.4	80.4
-3 dB (nominal)	3.4	17.9	86.1
-6 dB (nominal)	1.7	10.3	86.5
-9 dB (nominal)	.9	6.4	87.6
8.4:			
Saturation	12.3	37.0	80.9
-3 dB (nominal)	6.2	27.2	85.0
-6 dB (nominal)	2.9	15.0	85.2
-9 dB (nominal)	1.6	9.0	85.7
9.6			
Saturation	7.8	28.1	82.7
-3 dB (nominal)	4.3	19.9	84.5
-6 dB (nominal)	2.0	11.1	85.6
-9 dB (nominal)	.85	5.7	87.7
Direct-current beam	-----	----	90.7

TABLE 10. - RESULTS FOR MDC 1WX4 WITH MODIFIED REFOCUSING SYSTEM AND SECONDARY ELECTRON SUPPRESSION - TWO-STAGE CONFIGURATION OPTIMIZED AT 4.8 GHz (SATURATION)

Frequency, GHz	Fundamental efficiency, percent		Collector efficiency, η_c, percent
	Without MDC	With MDC	
4.8:			
Saturation	7.4	24.7	82.0
-3 dB (nominal)	3.7	19.5	86.3
-6 dB (nominal)	1.8	11.6	87.3
-9 dB (nominal)	.9	7.1	88.0
8.4:			
Saturation	12.3	36.3	80.5
-3 dB (nominal)	6.5	28.5	84.8
-6 dB (nominal)	3.2	17.5	85.9
-9 dB (nominal)	1.6	9.7	86.6
9.6:			
Saturation	8.0	29.4	83.7
-3 dB (nominal)	4.0	19.6	85.5
-6 dB (nominal)	2.0	11.6	86.2
-9 dB (nominal)	.95	6.5	87.7
Direct-current beam	-----	----	91.6

TABLE 11. - RESULTS FOR MDC 1WX4 WITH MODIFIED REFOCUSING SYSTEM AND SECONDARY ELECTRON SUPPRESSION - FOUR-STAGE CONFIGURATION OPTIMIZED AT 8.4 GHz (SATURATION)

Frequency, GHz	Fundamental efficiency, percent		Collector efficiency, η_c, percent
	Without MDC	With MDC	
4.8:			
Saturation	7.3	24.7	82.0
-3 dB (nominal)	3.6	19.4	86.5
-6 dB (nominal)	1.8	11.3	87.3
-9 dB (nominal)	.9	6.6	88.5
8.4:			
Saturation	12.6	39.8	83.3
-3 dB (nominal)	6.3	28.5	85.5
-6 dB (nominal)	3.1	17.3	86.3
-9 dB (nominal)	1.5	9.5	87.5
9.6:			
Saturation	8.1	30.5	84.2
-3 dB (nominal)	4.0	20.5	86.1
-6 dB (nominal)	2.1	12.4	86.8
-9 dB (nominal)	1.0	7.2	88.3
Direct-current beam	----	----	90.1

TABLE 12. - RESULTS FOR MDC 1WX4 WITH MODIFIED REFOCUSING SYSTEM AND SECONDARY ELECTRON SUPPRESSION - FOUR-STAGE CONFIGURATION OPTIMIZED AT 4.8 GHz (SATURATION)

Frequency, GHz	Fundamental efficiency, percent		Collector efficiency, η_c, percent
	Without MDC	With MDC	
4.8:			
Saturation	7.4	26.8	83.9
-3 dB (nominal)	4.3	20.8	87.4
-6 dB (nominal)	2.1	13.5	88.0
-9 dB (nominal)	.9	7.2	89.1
8.4:			
Saturation	12.5	37.9	81.4
-3 dB (nominal)	6.3	29.3	86.0
-6 dB (nominal)	3.2	18.6	87.2
-9 dB (nominal)	1.6	11.0	88.3
9.6:			
Saturation	8.0	30.5	84.3
-3 dB (nominal)	4.0	21.5	86.9
-6 dB (nominal)	2.1	13.5	88.0
-9 dB (nominal)	1.0	7.7	89.1
Direct-current beam	----	----	90.9

TABLE 13. - RESULTS FOR MDC 1WX5 WITH MODIFIED REFOCUSING SYSTEM AND SECONDARY ELECTRON SUPPRESSION - TWO-STAGE CONFIGURATION

Optimization frequency, GHz	Frequency, GHz		
	4.8	8.4	9.6
	Collector efficiency, η_c, percent		
4.8 (saturation)	82.4	80.2	83.4
8.4 (saturation)	81.1	82.1	83.3

TABLE 14. - RESULTS FOR MDC 1WX5 WITH MODIFIED REFOCUSING SYSTEM AND SECONDARY ELECTRON SUPPRESSION - TWO-STAGE CONFIGURATION OPTIMIZED AT 8.4 GHz (SATURATION)

Frequency, GHz	Fundamental efficiency, percent	Collector efficiency, η_c, percent
4.8:		
Saturation	23.2	81.1
-3 dB	17.5	85.8
-6 dB	10.1	86.1
8.4:		
Saturation	39.0	82.1
-3 dB	27.5	84.5
-6 dB	16.9	85.1
9.6:		
Saturation	30.7	83.3
-3 dB	20.4	84.9
-6 dB	12.1	85.4
Direct-current beam	----	90.1

TABLE 15. - RESULTS FOR MDC 1WX5 WITH MODIFIED REFOCUSING SYSTEM AND SECONDARY ELECTRON SUPPRESSION - FOUR-STAGE CONFIGURATION

Optimization frequency, GHz	Frequency, GHz		
	4.8	8.4	9.6
	Collector efficiency, η_c, percent		
4.8 (saturation)	84.8	82.0	85.4
8.4 (saturation)	83.2	84.2	85.2
Compromise optimization	83.8	83.6	85.3

TABLE 16. - RESULTS FOR MDC 1WX5 WITH MODIFIED REFOCUSING SYSTEM AND SECONDARY ELECTRON SUPPRESSION - FOUR-STAGE CONFIGURATION OPTIMIZED TO GIVE MORE UNIFORM COLLECTOR EFFICIENCY

Frequency, GHz	Fundamental efficiency, percent	Collector efficiency, η_c, percent
4.8:		
Saturation	25.4	83.8
-3 dB (nominal)	20.1	87.7
-6 dB (nominal)	12.1	88.3
-9 dB (nominal)	7.0	89.3
8.4:		
Saturation	40.5	83.6
-3 dB (nominal)	30.8	86.7
-6 dB (nominal)	19.4	87.9
-9 dB (nominal)	11.3	88.7
9.6:		
Saturation	32.0	85.3
-3 dB (nominal)	24.8	87.1
-6 dB (nominal)	14.3	88.0
-9 dB (nominal)	8.6	89.3
Direct-current beam[a]	----	91.5

[a]The upper limit of direct-current beam collection efficiency is given by the ratio of the potential of the plate next to the cone, i. e., -8.87 kV in this case, to the cathode potential -9.45 kV.

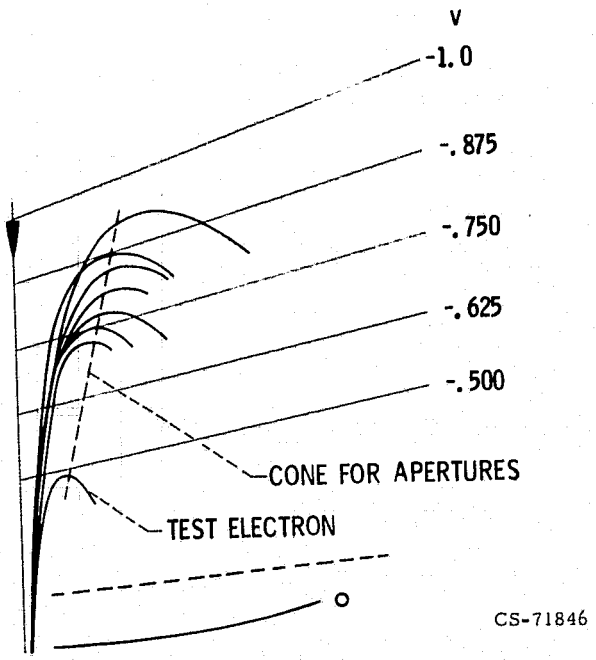

Figure 1. - Actual electron trajectories for average injection angles.

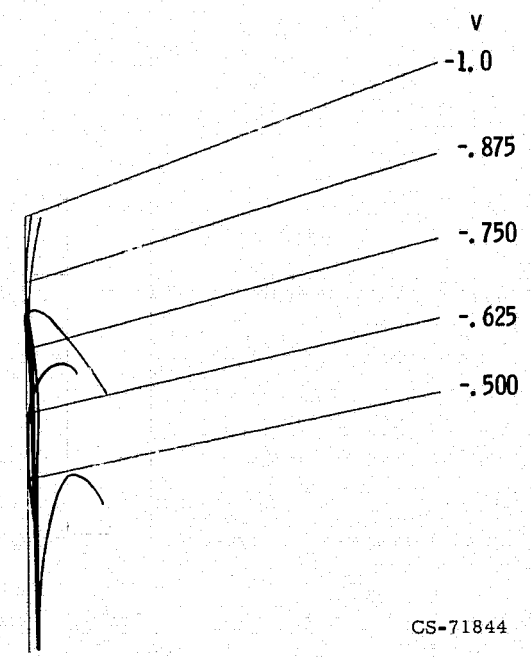

Figure 2. - Actual electron trajectories for small negative injection angles.

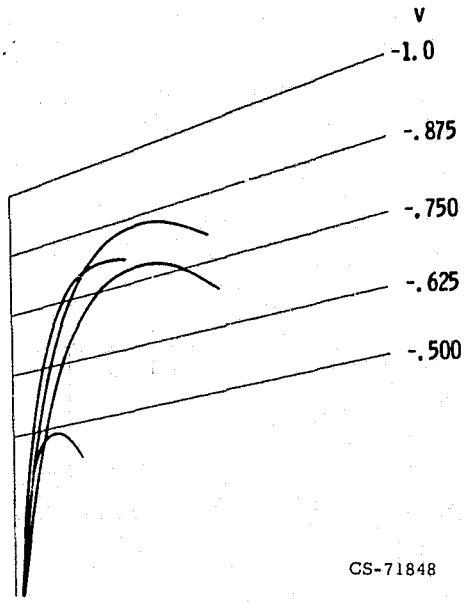

Figure 3. - Actual electron trajectories for large positive injector angles.

$(B_C = 0, \ddot{r} = 0)$

1. BUSCH'S THEOREM

$$\dot{\varphi} = \frac{e}{2m} B_Z$$

2. ADIABATIC BEAM EXPANSION

$$\frac{r_1}{r_0} = \frac{B_{Z0}}{B_{Z1}}$$

3. ELECTRON DIPOLE MOMENT

$$(\dot{r}^2 + r^2\dot{\varphi}^2)^{1/2} r^2 = \text{CONST}$$

RADIAL VELOCITY REDUCTION

$$\dot{r}_1^2 \approx \dot{r}_0^2 \left(\frac{B_{Z1}}{B_{Z0}}\right)^4 - r_0^2\dot{\varphi}_0^2 \left[1 - \left(\frac{B_{Z1}}{B_{Z0}}\right)^4\right]$$

CS-71864

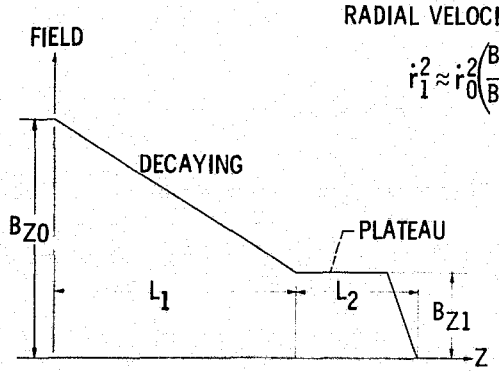

(a) SCHEMATIC OF THE SPENT BEAM REFOCUSING SYSTEM.

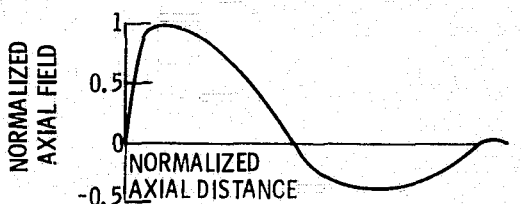

(b) REFOCUSING FIELD WITH REVERSAL.

Figure 4.

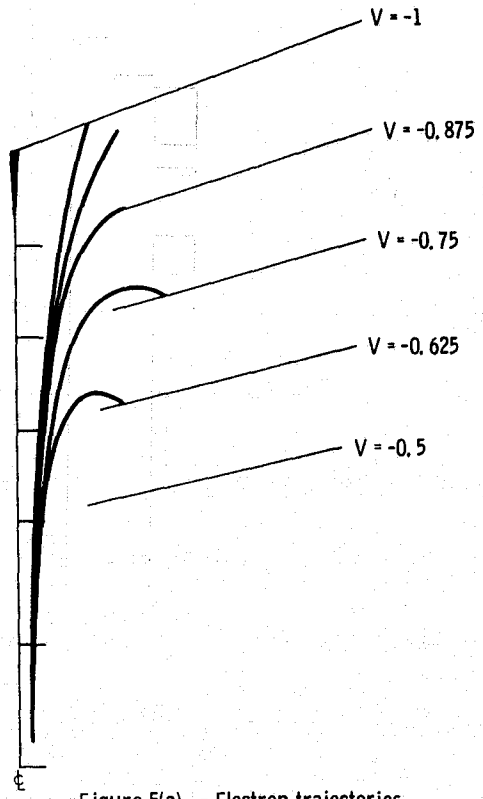

Figure 5(a). - Electron trajectories.

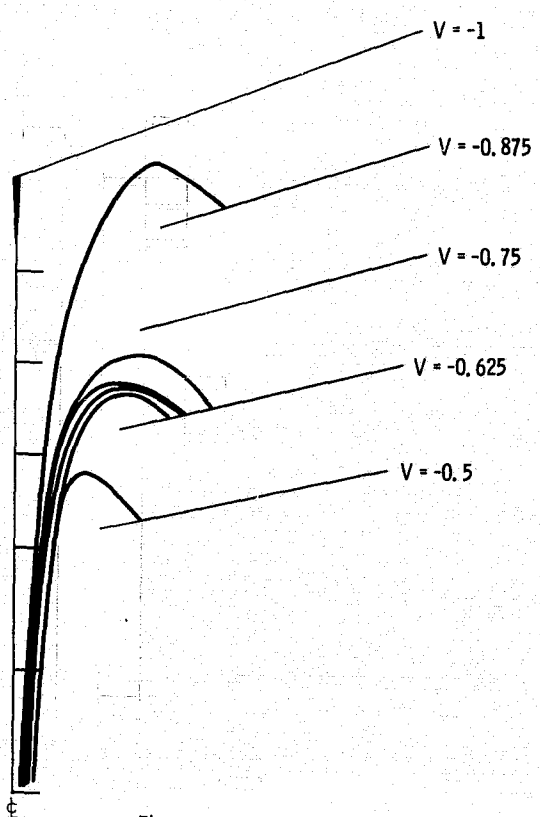

Figure 5(b). - Continued.

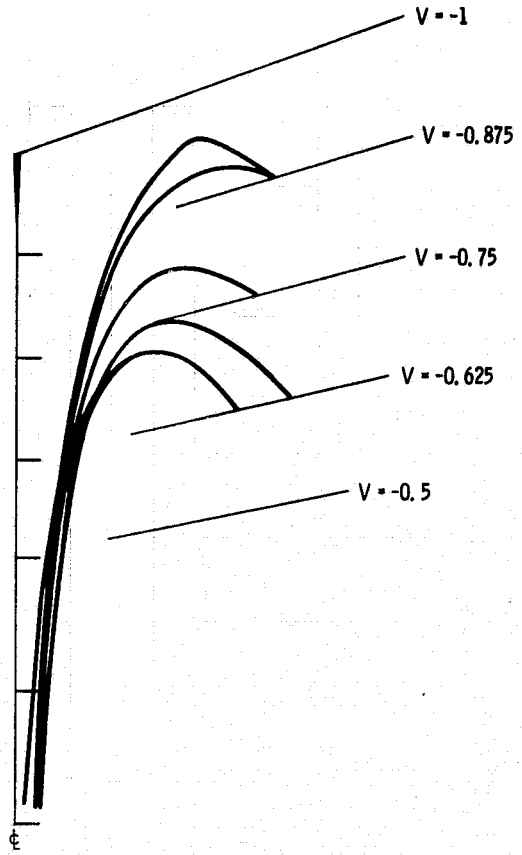

Figure 5(c). - Continued.

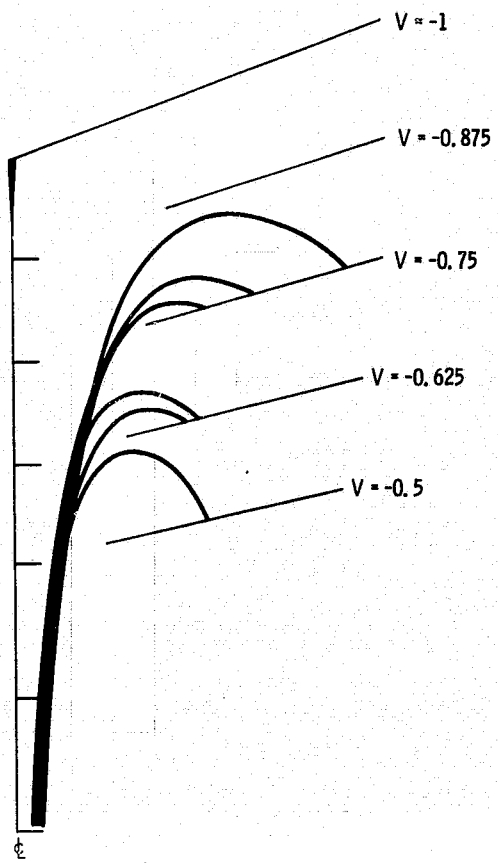

Figure 5(d). - Continued.

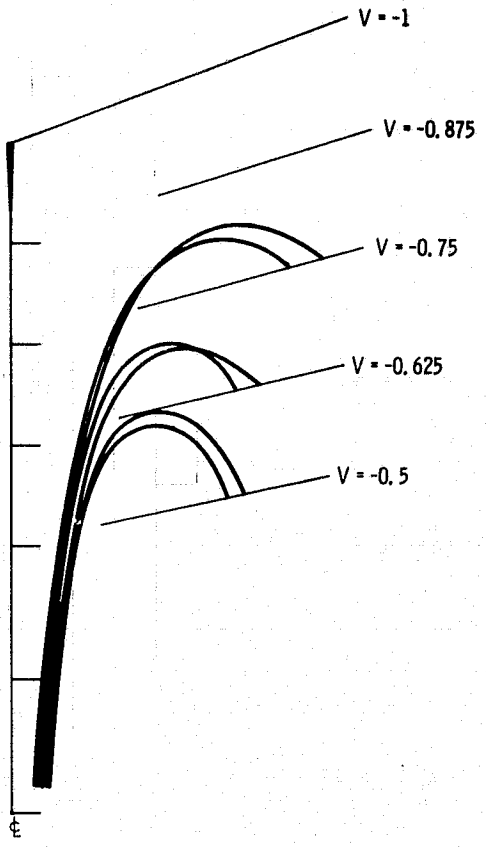

Figure 5(e). - Continued.

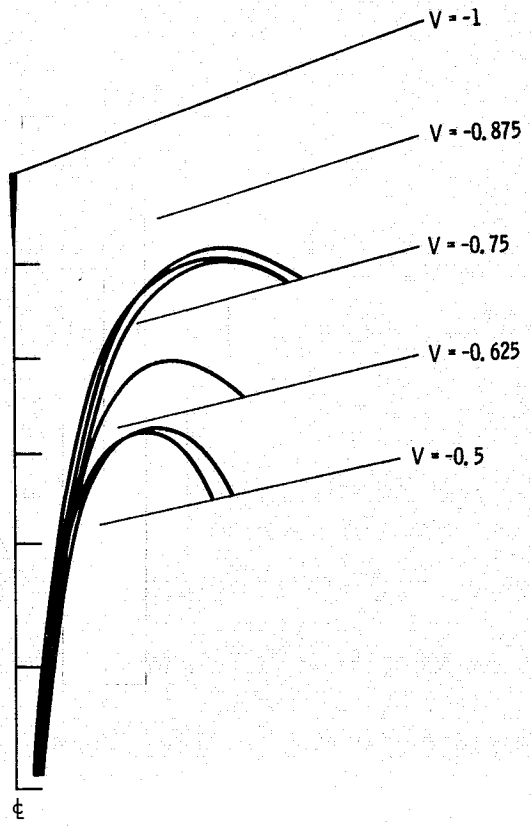

Figure 5(f). - Concluded.

	%
1. FINITE NO. OF ELECTRODES (2-4) COMPARED WITH INFINITE NO.	10-5
2. RADIAL VELOCITY SORTING	3
3. VERY LARGE ANGLES ($\geq 6^0$) & VERY SMALL ANGLES ($\leq 0.25^0$)	2-4
4. SECONDARIES ON CONE & ELSEWHERE	2.7-4.7
5. ASYMMETRY & NONCIRCULARITY OF THE BEAM*	
6. NONIDEAL TUBES*	
7. NO REFOCUSING AT ALL	9

*RANGE CAN VARY WIDELY

Figure 6. - Analysis of collector inefficiency with good refocusing and no secondary suppressing coating for 10-20 percent efficient TWTs.

FOR $\eta_{CT} < 1$

$$\eta_o = \frac{\eta_{CT} \cdot \eta_e}{1 - \eta_c + \eta_e \eta_c}$$

η_e = ELECTRONIC
η_c = COLLECTOR
η_{CT} = CIRCUIT
η_o = OVERALL
} EFFICIENCY

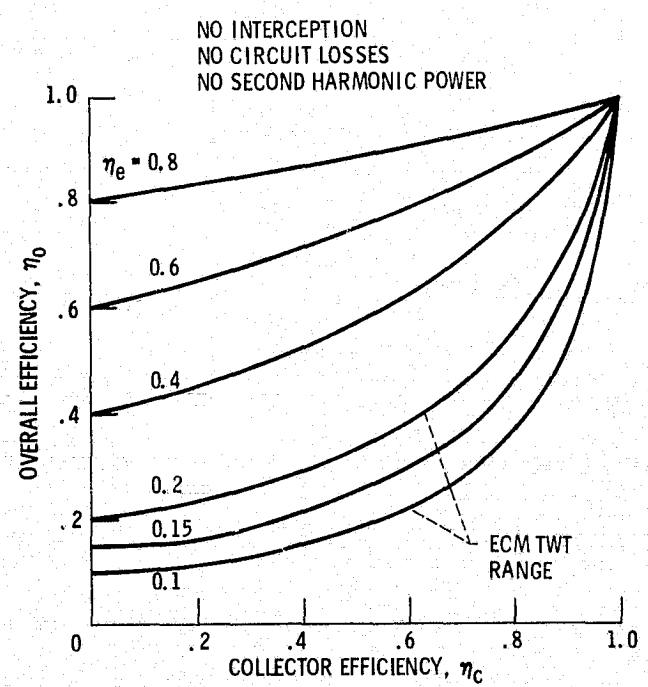

Figure 7(a). - Overall efficiency vs. collector efficiency.

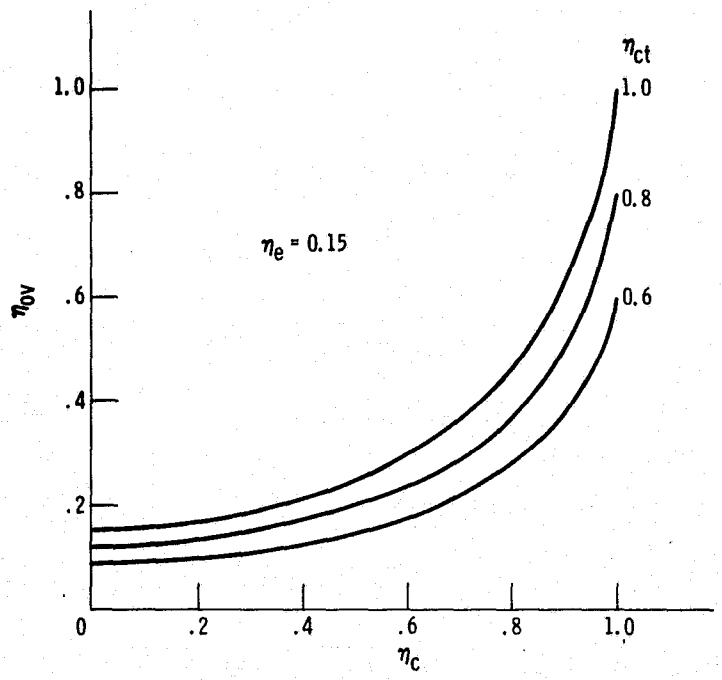

Figure 7(b). - Effect of circuit losses on the overall tube efficiency for $\eta_e = 0.15$.

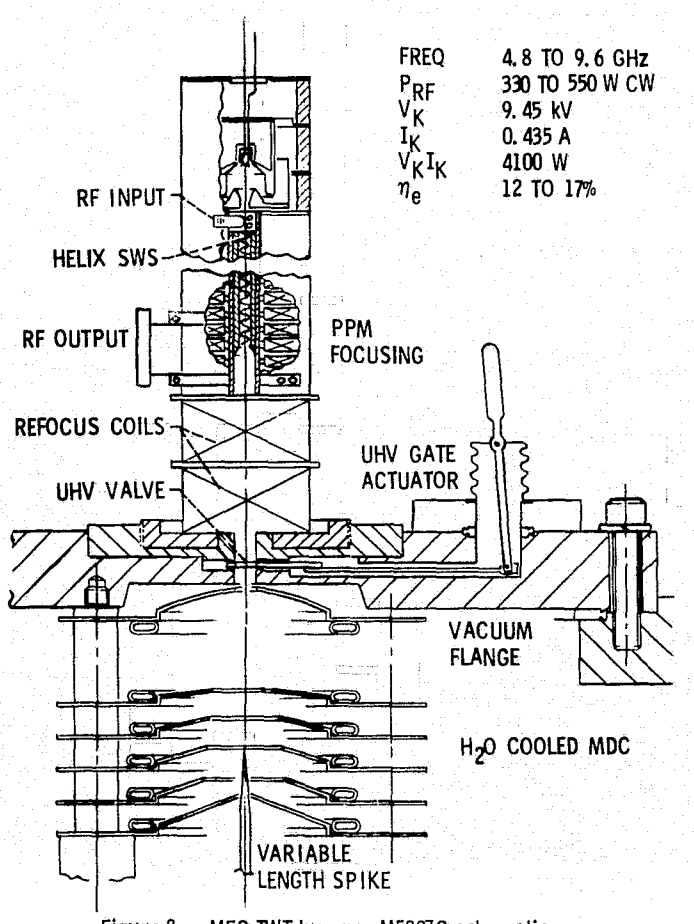

Figure 8. - MEC TWT typ. no. M5897C schematic.

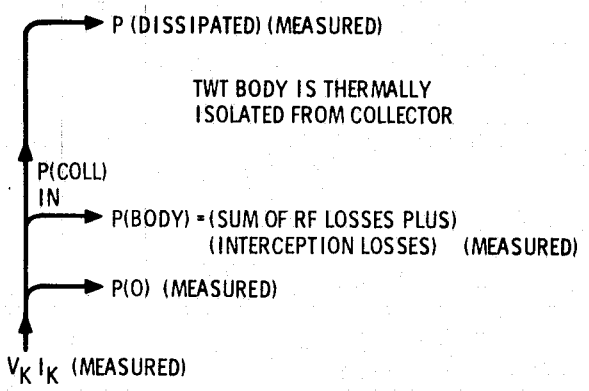

Figure 9(a). - Power flow diagram TWT with undepressed collector (bench test).

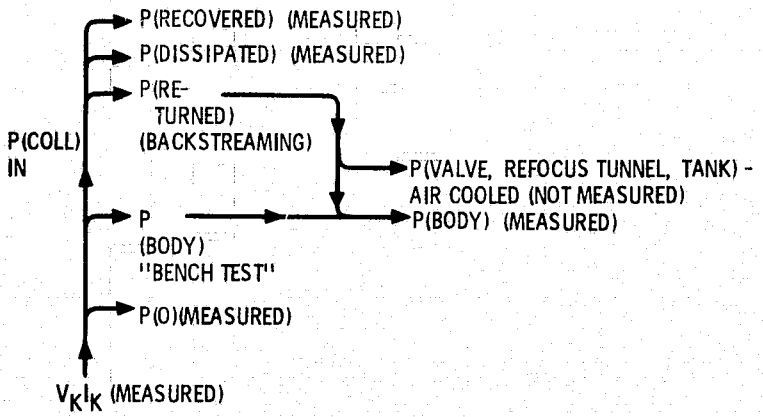

Figure 9(b). - Power flow diagram TWT with LeRC MDC.

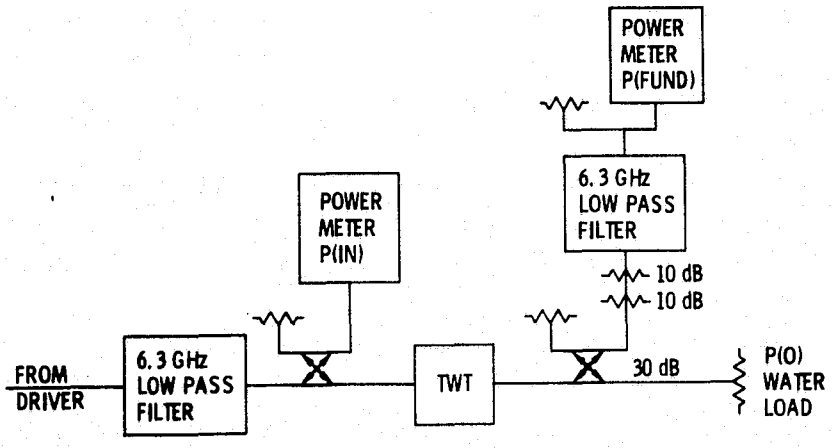

RF TEST SETUP FOR FREQ. < 6.4 GHz

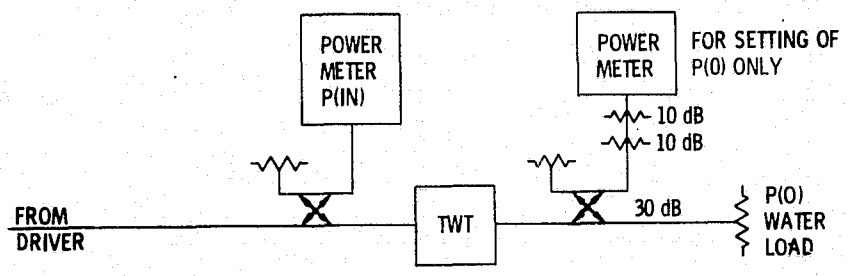

RF TEST SETUP FOR FREQ. ≥ 6.4 GHz

Figure 10.

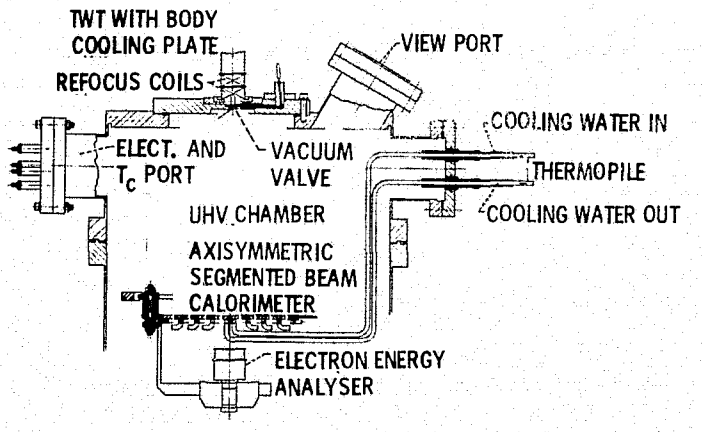

Figure 11. - Schematic of the spent beam measuring set-up.

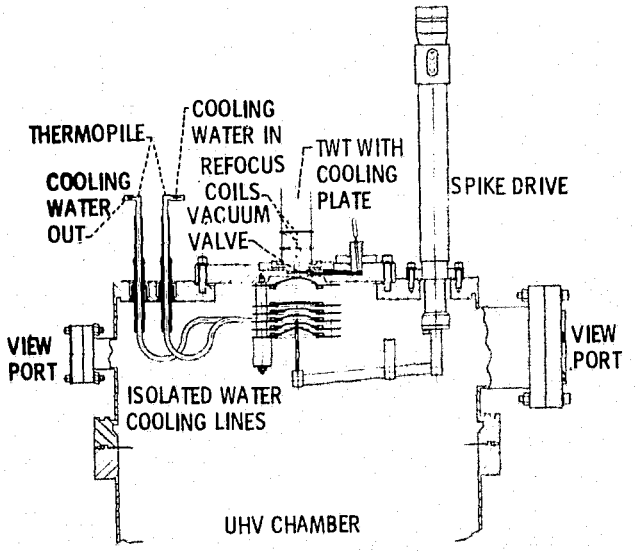

Figure 12. - Schematic of the MDC measuring system.

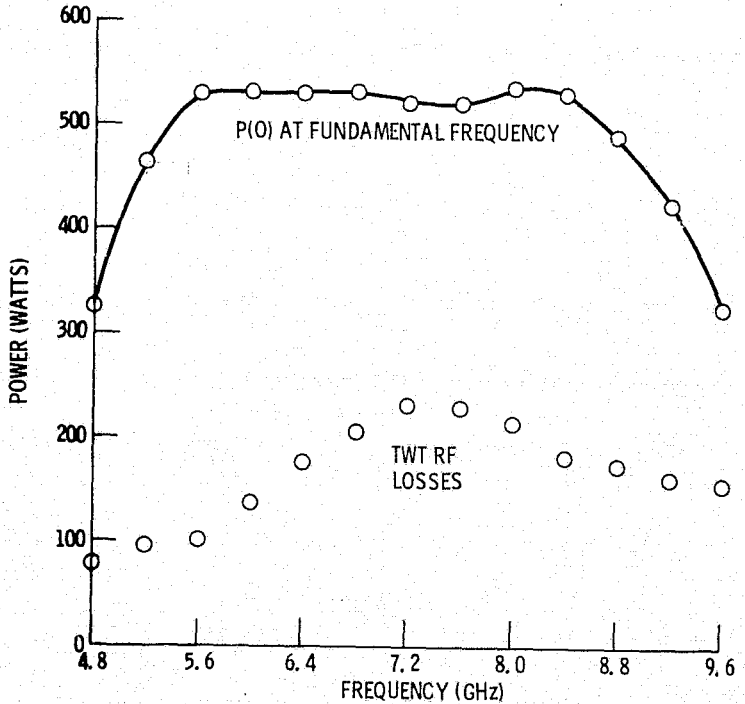

Figure 13. - $P_{(FUND)}$ and $P_{RF\ LOSSES}$ versus frequency.

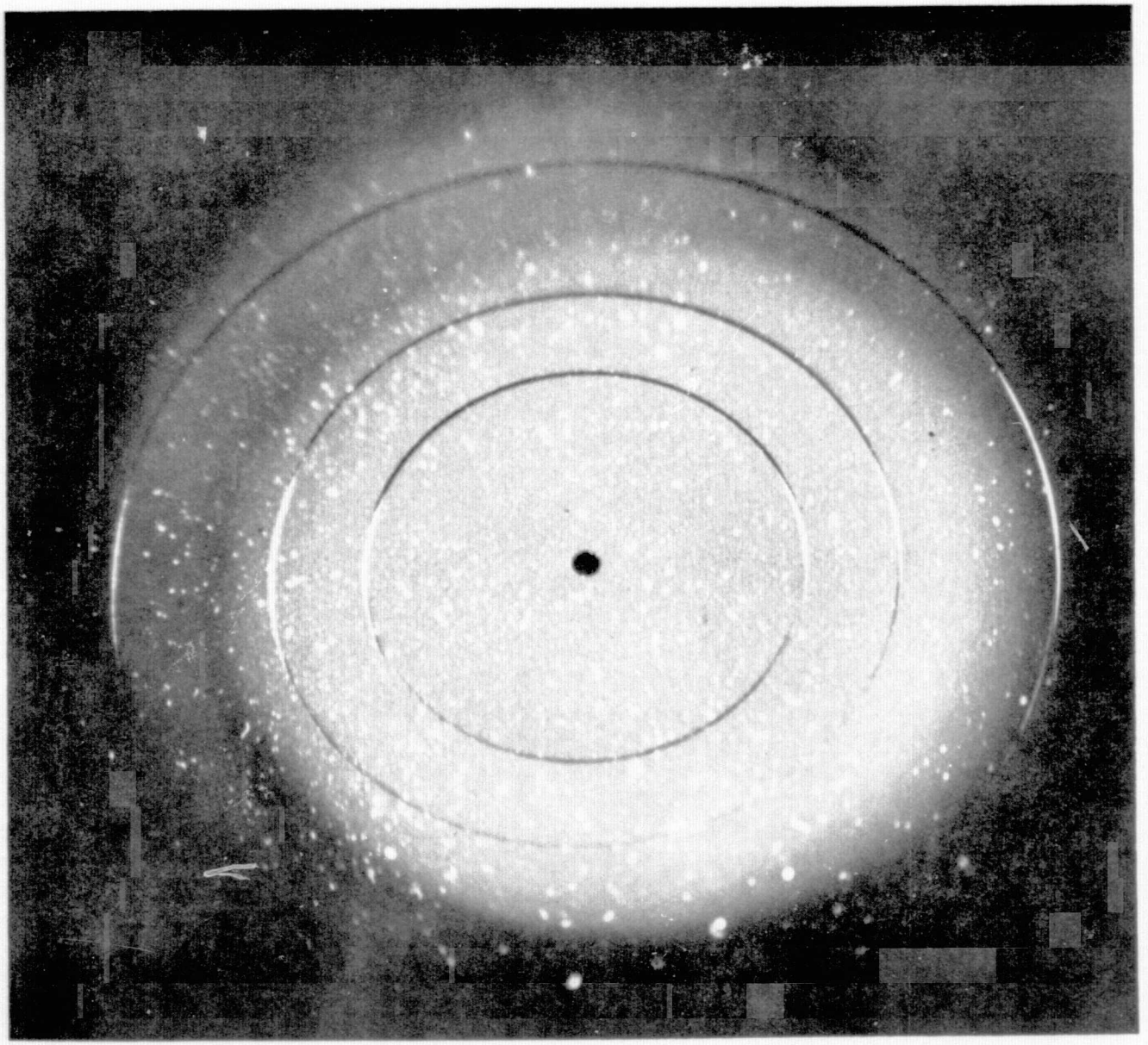

Figure 14. - Spent beam cross-section after refocusing.

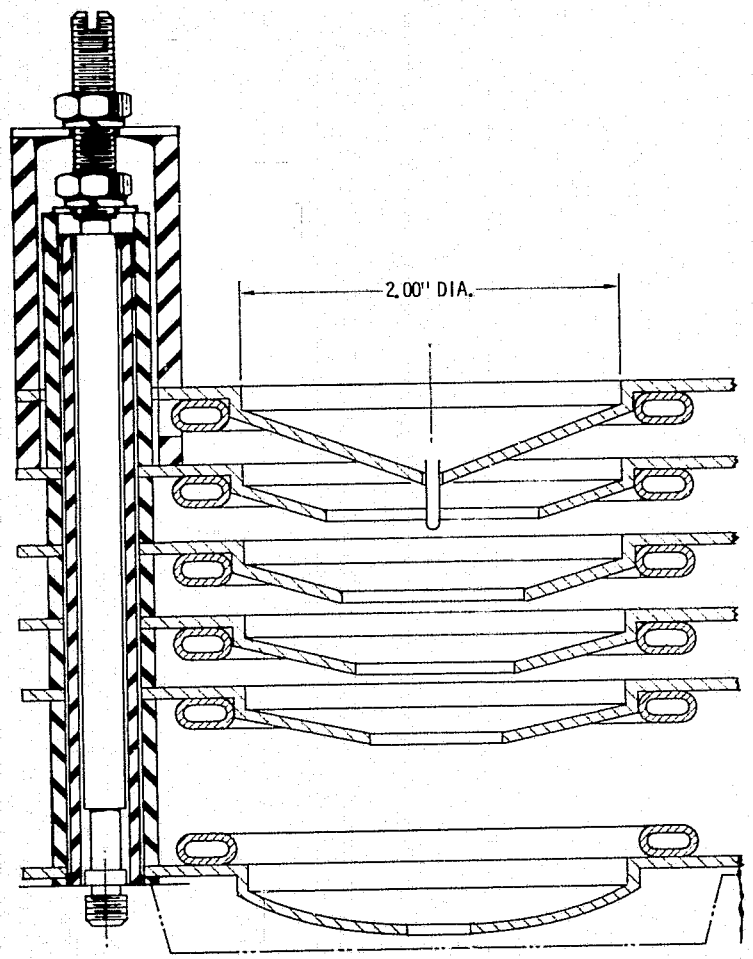

Figure 15. - MDC 1W.

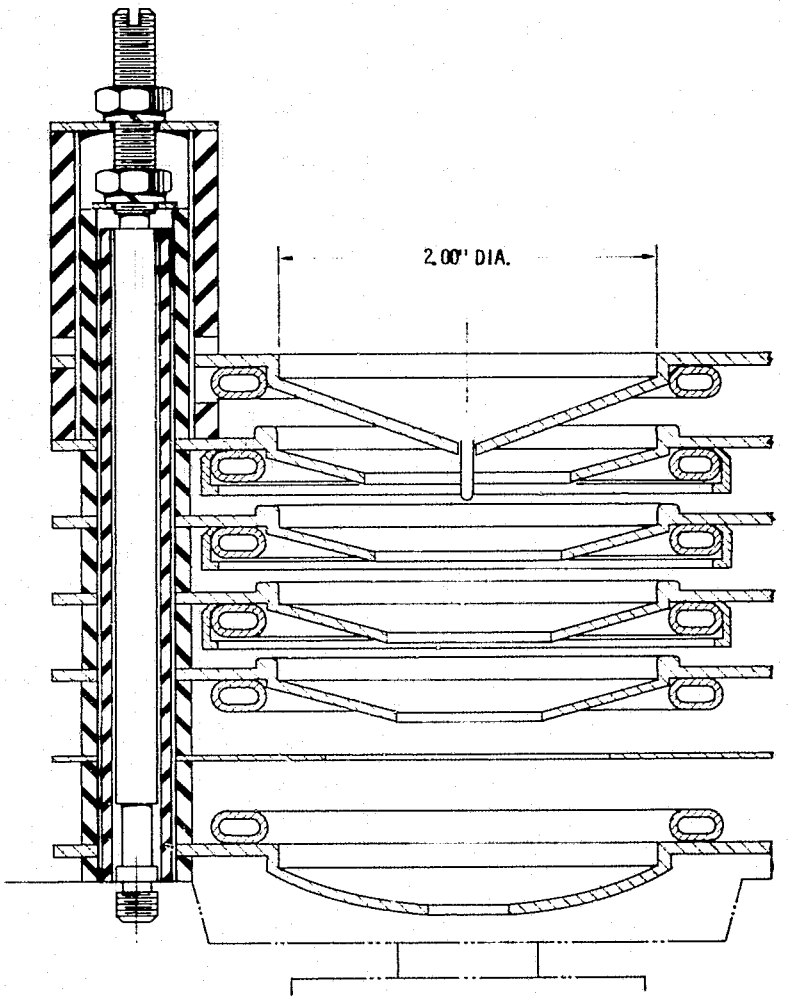

Figure 16. - MDC 1Wx1.

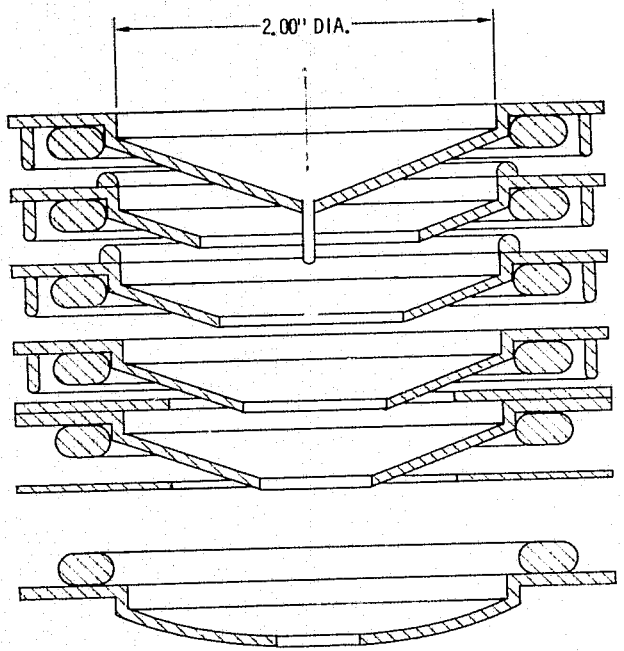

Figure 17. - MDC 1Wx3.

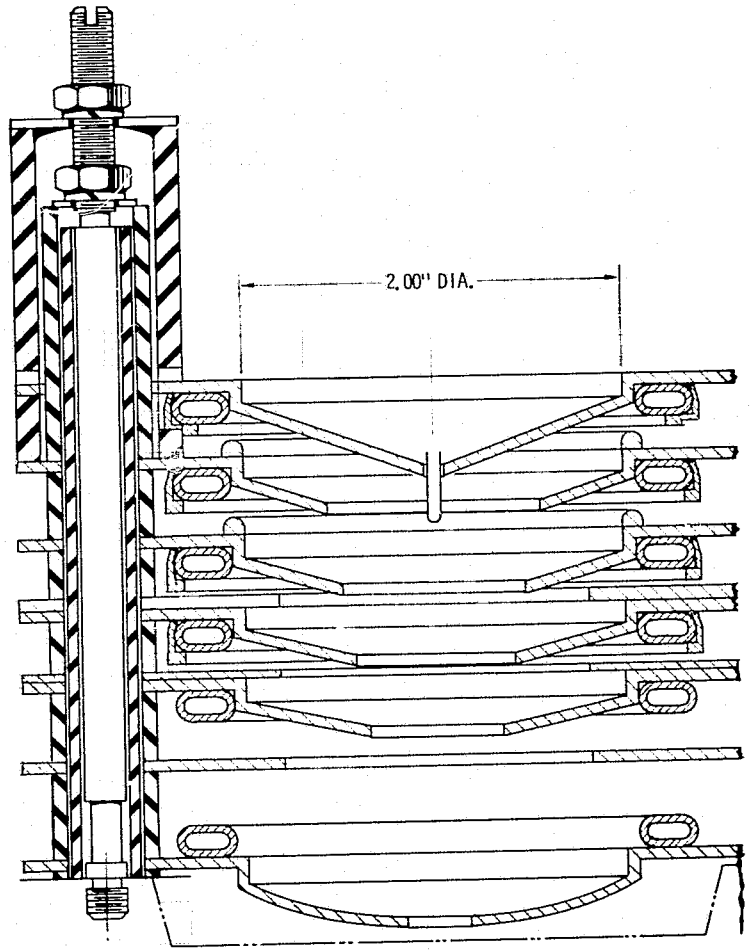

Figure 18. - MDC 1Wx4.

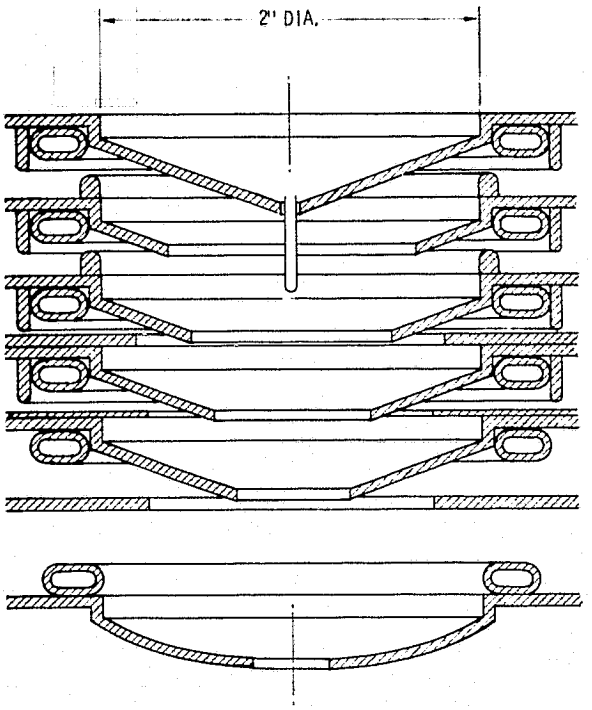

Figure 19. - MDC 1Wx5.